

Unraveling the Autism spectrum heterogeneity: Insights from ABIDE I Database using data/model-driven permutation testing approaches

F.J. Alcaide^a, I.A. Illan^a, J. Ramírez^a, J.M. Gorriz^{a,b,c,*}

^a*DaSCI Institute, University of Granada, Spain*

^b*Dpt. of Psychiatry, University of Cambridge, UK*

^c*ibs.Granada, Granada, Spain*

Abstract

Autism Spectrum Condition (ASC) is a neurodevelopmental condition characterized by impairments in communication, social interaction and restricted or repetitive behaviors. Extensive research has been conducted to identify distinctions between individuals with ASC and neurotypical individuals. However, limited attention has been given to comprehensively evaluating how variations in image acquisition protocols across different centers influence these observed differences. This analysis focuses on structural magnetic resonance imaging (sMRI) data from the Autism Brain Imaging Data Exchange I (ABIDE I) database, evaluating subjects' condition and individual centers to identify disparities between ASC and control groups. Statistical analysis, employing permutation tests, utilizes two distinct statistical mapping methods: Statistical Agnostic Mapping (SAM) and Statistical Parametric Mapping (SPM). Results reveal the absence of statistically significant differences in any brain region, attributed to factors such as limited sample sizes within certain centers, nuisance effects and the problem of multicentrism in a heterogeneous condition such as autism. This study indicates limitations in using the ABIDE I database to detect structural differences in the brain between neurotypical individuals and those diagnosed with ASC. Furthermore, results from the SAM mapping method show greater

*Corresponding author

Email address: gorriz@ugr.es (J.M. Gorriz)

consistency with existing literature.

Keywords: Statistical parametric mapping, linear support vector machines, statistical learning theory, permutation tests, Magnetic Resonance Imaging, Upper Bounding.

1. Introduction

ASC, also referred to as autism, is a neurodevelopmental disorder with significant implications for communication, social interaction, and behavioral patterns [35, 38, 58]. The disorder exhibits a complex nature, encompassing a broad spectrum of symptoms and severity levels, thereby posing challenges in terms of diagnosis and treatment [25]. In the previous edition of the American Psychiatric Association’s Diagnostic and Statistical Manual of Mental Disorders (DSM-IV) [8], autism was categorized into five distinct subtypes: Autistic Disorder, Rett Syndrome, Asperger Syndrome, Childhood Disintegrative Disorder, and Pervasive Developmental Disorder Not Otherwise Specified. However, the fifth edition of the DSM (DSM-5) introduced updated recommendations for the classification of ASC. Presently, the diagnostic range for ASC is unified under a single spectrum, eliminating the subtypes. The DSM-5 [6] incorporates a generalized ASC category, omitting Rett Syndrome and Childhood Disintegrative Disorder. This revised classification framework, centered on a unified spectrum, aims to improve the comprehensive representation of the diverse manifestations observed in ASC. It also facilitates the diagnosis of cases characterized by subtle yet intrinsic features of the disorder. Consequently, individuals with ASC, including those with milder phenotypes, can gain access to tailored therapies aligned with their specific requirements.

The long-term consequences of ASC exhibit increased severity, contributing to a higher susceptibility of affected individuals to medical complications [27]. Additionally, ASC demonstrates a significant gender imbalance, with male-to-female ratios of 1.8:1 in adults and 3.5:1 in children and adolescents [52]. Nonetheless, our understanding of the inherent cerebral distinctions be-

tween neurotypical individuals and those with ASC remains limited. Efforts have been made over the years to address this knowledge gap [14], prompting researchers to employ neuroimaging methodologies for investigating the structural and functional aspects of the brain in individuals with ASC [60].

1.1. Related Works

Within the existing literature, a considerable number of research papers have focused on investigating the anatomical differences in the brains of individuals with autism compared to neurotypical individuals [50, 11, 48]. These studies aim to identify specific brain regions that exhibit significant differences, striving to achieve a high level of accuracy in identifying and understanding the neurological characteristics associated with autism [2].

Studies such as the one conducted by Segovia et al. [54], the focus was on identifying differences among three distinct groups: control participants, individuals with ASC, and unaffected siblings of individuals with ASC. They employed a univariate methodology using magnetic resonance images (MRI), combining a reflector approach and a support vector machines (SVM) classifier to detect differences between the groups.

McAlonan et al. [39] conducted a comprehensive voxel-based volumetric analysis of the entire brain using automated techniques. They compared children with ASC to typically developing (TD) children. The findings of the study indicated abnormalities in the anatomy and connectivity of the limbic-striatal brain systems. These observed abnormalities may contribute to differences in brain metabolism and contribute to the behavioral characteristics associated with autism.

Gori et al. [21] conducted sMRI analysis of children with ASC and healthy control (HC) using Statistical Parametric Mapping (SPM) and Freesurfer to extract morphometric brain information, and a SVM classifier to localize the brain regions contributing to classification.

Li et al. [33] analyzed grey matter (GM) volume in children with ASC compared to HC, particularly focusing on children with Low Functioning Autism

(LFA) [34], obtaining findings regarding a reduction in GM volume in several brain regions.

2. Machine learning methods in ASC

Classical machine learning (ML) algorithms have extensively been used to extract distinctive features from neuroimages in order to discern variations between subjects[15]. Several studies have utilized voxel-based morphometry (VBM) [5] to examine and compare total brain volume (TBV) and regional disparities in individuals with ASC [12]. In [51], it was observed that TBV and gray matter volumes increased by 1-2% in individuals with ASC. However, this finding only attained statistical significance when the entire dataset was considered, without matching the images by age and sex. A common finding in [47, 46, 45] is the identification of a significantly larger median sagittal brain area in individuals with ASC compared to control subjects. Furthermore, these studies indicated that the increase in brain volume [32] is not a uniform phenomenon but varies across the frontal, temporal, parietal, and occipital lobes. In contrast, [7] reported no discernible differences in brain volume among subjects older than 12 years. However, an increase in head circumference was observed in individuals with ASC, leading to the conclusion that it stemmed from an expansion in brain volume during childhood.

In [23], a partial least squares feature extractor was employed to demonstrate disparities in regional brain structure between genders and neurological conditions. The study highlighted the influence of gender on ASC, even when utilizing a balanced dataset for classification. Similarly, [64] investigated age and gender dependencies using volumes of GM, white matter (WM), and subcortical structures, yielding positive outcomes.

Other diverse approaches encompassed surface-based morphometry (SBM) [26], analysis of words and phrases from children’s assessments [36], and the utilization of multiple SVM [10, 37] to enhance the final classification [9]. In [2], a computer-aided diagnosis (CAD) system was developed, involving the

extraction of the cerebral cortex from sMRI and the creation of personalized neuroatlases that describe specific developmental patterns of the autistic brain.

2.1. Novel Advances in neuroimaging based on ML

Similar to classical analysis approaches, neural networks have been utilized to leverage structural and functional connectivity patterns for the classification of individuals with ASC. The Autism Brain Imaging Data Exchange I (ABIDE I) dataset was employed as a common database in these studies. In [24], subjects were classified based on their brain activation patterns, achieving a 70% accuracy in identifying patients with ASC compared to controls. In [56], the focus was on automatic detection of ASC using Convolutional Neural Network (CNN) with a brain imaging dataset consisting of resting-state functional magnetic resonance imaging (fMRI) data. The model successfully classified subjects based on patterns of functional connectivity, achieving an accuracy of 70.22% in detecting ASC. [62] implemented a design incorporating four distinct hidden layer configurations of Deep Neural Network (DNN) models to classify ASC from TD individuals. The model achieved an accuracy of 75.27%, recall of 74%, and precision of 78.37%. In [30], individual brain networks were constructed for each subject, and a DNN classifier was employed with the input consisting of the 3000 most relevant features. The results demonstrated an accuracy of 90.39% and an area under the receiver operating characteristic curve (AUC) of 0.9738 for ASC/TD classification. Ms et al. [41] introduced DarkASDNet, a new approach utilizing fMRI data for predicting the binary classification between ASC and TD in the ABIDE-I, NYU dataset. The proposed method achieved state-of-the-art accuracy of 94.70% in the classification task. In [55], a grid search optimization (GSO) algorithm was applied to optimize hyperparameters in Deep Convolutional Neural Networks (DCNN) used in the system. As a result, the proposed diagnostic method based on sMRI achieved an exceptional success rate of 100% in identifying ASC.

In [29], the authors investigated the impact of stochastic parcellations of the brain by employing an ensemble architecture in conjunction with a CNN. This

approach facilitated the combination of predictions from different parcellations. Temporal and spatial information from fMRI images were leveraged in [63]. A sliding window technique was applied to create two-channel images, which served as the input to a CNN. This enabled the exploration of dynamic patterns in the data. Zhao et al. [65] introduced an effective 3D CNN framework that derived discriminative and significant spatial brain network overlap patterns. This framework proved valuable for distinguishing between individuals with ASC and TD.

In recent advancements of deep learning for neuroimaging, particular attention has been given to Graph Convolutional Network (GCN). These networks enable classification not only at the individual level but also consider the relationships within the entire population of data. In [4, 49], the combination of functional and structural MRI information was employed to enhance the classification performance. Accuracies of 64.23% and 85.06% were achieved, respectively. Specifically, [4] utilized the fusion of information to construct the edges and nodes of the GCN. Furthermore, in [3], an ensemble of weakly trained GCNs was utilized to enhance performance robustness against architectural changes. This approach aimed to improve the overall stability and reliability of the classification results. Through the implementation of this method, an accuracy of 70.86% was achieved.

This paper aims to investigate the structural MRI data within the multicenter and international ABIDE I database [13], focusing on its relevance to characterizing autism. It examines patients in a comprehensive manner based on their condition, as well as investigates each center individually. The analysis will employ rigorous statistical methodologies, including a permutations test, and two established neuroimaging mapping techniques, namely Statistical Agnostic Mapping (SAM) [22] and SPM [18, 43]. The primary objective is to identify and validate any brain regions demonstrating significant differences between individuals diagnosed with autism and healthy controls. Furthermore, the study underscores the inherent challenges posed by highly heterogeneous data within multicenter databases like ABIDE, particularly in the context of

analyzing a disorder as diverse as autism[40].

3. Materials and Methods

3.1. ABIDE I dataset

Comprehensive and extensive datasets are required to further our understanding of the underlying brain mechanisms associated with autism and the intricate and heterogeneous nature of the disorder. To address this need, the ABIDE I initiative was established. ABIDE I aims to collect functional and structural brain imaging data from multiple research laboratories worldwide, providing a valuable resource for advancing our knowledge of ASC.

The ABIDE I database comprises magnetic resonance images shared by 20 international centers. For our analysis, we accessed a dataset consisting of 1032 images, with 527 images corresponding to HC and 505 images representing individuals with ASC, as summarized in Table 1. The brain images of each subject sourced from the ABIDE I database underwent preprocessing and segmentation procedures, with only the complete GM map of each image being utilized. Subsequently, the brain volumes were partitioned into 116 regions of interest (ROI) using a brain atlas established by the Automated Anatomical Labeling (AAL) method [59]. Within the article [57], there is a table (Table 2) which provides the names and corresponding numbers, according to the predefined AAL order, of the 116 ROI that are employed in the study.

3.2. Preprocessing and outliers detection

The MRI images obtained from the ABIDE I database were subjected to processing and segmentation using the SPM software. While SPM was primarily developed for functional imaging, it also offers functionalities for spatial realignment, smoothing, and normalization in the standard T1-weighted image space. The entire process was conducted utilizing the VBM Toolbox within SPM [1]. The preprocessing steps, including co-registration and segmentation, as well as the specific parameters employed at each stage, can be summarized as follows:

Table 1: Number of brain images contributed by each center, categorized according to their condition, specifically control (HC) or autism (ASC).

Sites	HC	ASC
CALTECH	18 [14M/4F]	19 [15M/4F]
CMU	13 [10M/3F]	14 [11M/3F]
KKI	28 [20M/8F]	20 [16M/4F]
LEUVEN_1	15 [15M/0F]	14 [14M/0F]
LEUVEN_2	19 [14M/5F]	15 [12M/3F]
MAX_MUN	28 [27M/1F]	24 [21M/3F]
NYU	100 [74M/26F]	75 [65M/10F]
OHSU	15 [15M/0F]	13 [13M/0F]
OLIN	14 [14M/0F]	20 [17M/3F]
PITT	26 [22M/4F]	30 [26M/4F]
SBL	15 [15M/0F]	15 [15M/0F]
SDSU	22 [16M/6F]	14 [13M/1F]
STANFORD	17 [13M/4F]	18 [14M/4F]
TRINITY	25 [25M/0F]	22 [22M/0F]
UCLA_1	30 [27M/3F]	41 [35M/6F]
UCLA_2	13 [11M/2F]	13 [13M/0F]
UM_1	54 [37M/17F]	53 [45M/8F]
UM_2	21 [20M/1F]	13 [12M/1F]
USM	26 [26M/0F]	44 [44M/0F]
YALE	28 [20M/8F]	28 [20M/8F]

1. Preprocessing

- The process used tissue probability maps to guide the analysis. The International Consortium for Brain Mapping (ICBM) provide these maps, which are derived from 452 T1-weighted scans that were aligned with an atlas space, corrected for scan inhomogeneities, and classified into three tissue types: GM, WM, and Cerebrospinal Fluid (CSF). The resulting maps were used to estimate a nonlinear deformation field that best aligns the tissue probability maps with each individual subject's image. The images were resized to 79 x 95 x 79 voxels with voxel sizes of 2 mm (sagittal) x 2 mm (coronal) x 2 mm (axial).
- A mutual information affine registration with the tissue probability maps was used to achieve approximate alignment.
- Spatial normalization was based on a high-dimensional Dartel normalization and used standard Dartel template provided by VBM 8

2. Segmentation

- For each tissue class (GM, WM, CSF), the intensity distribution was represented using a certain number of Gaussians, 2 in this case. The use of multiple components per tissue allows to reckon partial volume effects and deep GM differing from cortical GM.
- A very light bias regularization was performed to correct smooth, spatially varying artifacts that modulates the intensity of the images.
- A spatial adaptive non local means denoising filter is applied to the data in order to remove noise while preserving edges. The smoothing filter size is automatically estimated based on the local variance in the image.
- Skull stripping was performed by using SPM-VBM tool and VBM templates.

As a result of the preprocessing and segmentation procedures, probability maps were generated for each MRI image in the database. These maps assigned

values within the range of 0 to 1 to each voxel, representing the probability of that voxel belonging to specific tissues, such as WM, GM, or CSF. However, for the purpose of our study, only the GM map derived from the images will be utilized.

3.3. Statistical Parametric Mapping

SPM, or Statistical Parametric Mapping [18, 43], is a neuroimaging tool that utilizes voxel-wise statistical analysis to examine and compare structural and functional brain data in relation to different conditions or tasks. The statistical analysis of MRI data employs a univariate mass approach based on General Linear Model (GLM). This approach entails the specification of a GLM design matrix, which in our case involves utilizing a two-sample t -test to divide the MRI images into two equally-sized groups. Subsequently, the model is estimated through the classical method, employing restricted maximum likelihood (ReML) to estimate the parameters. This estimation assumes that the error correlation structure is uniform across all voxels. Following the estimation, specific parameter profiles are subjected to testing using T statistics with contrasts assigned values of +1 and -1 for each respective image class. To mitigate the risk of false positive (FP) results in the context of multiple comparisons, a whole-brain cluster-level Family-wise Error (FWE) correction was applied, maintaining a significance level (α) of 0.05, rejecting the null hypothesis if $p < 0.05$. This correction technique helps ensure that only statistically significant findings are considered. Figure 1 presents a block diagram illustrating the analysis process with SPM, highlighting the main steps involved.

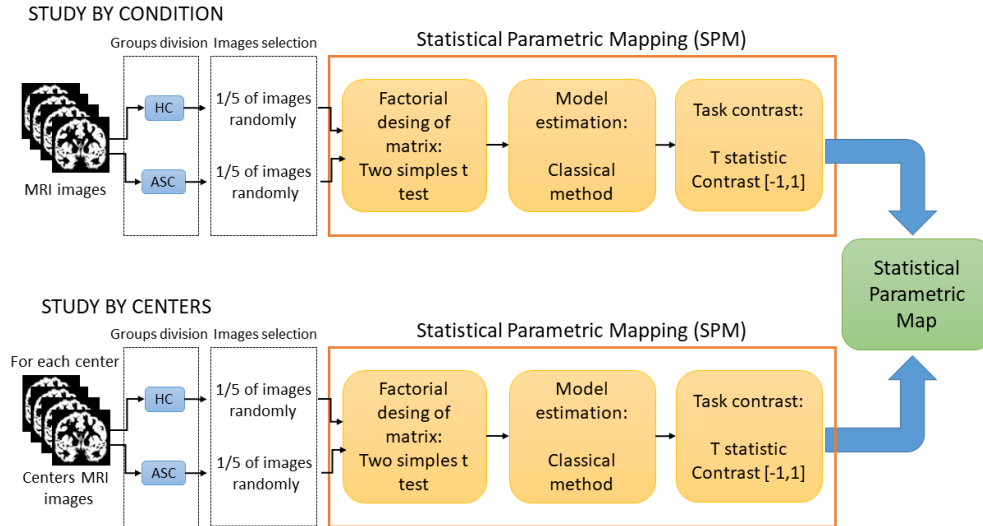


Figure 1: The block diagram illustrates the MRI analysis process using SPM and its three main steps. The diagram specifically focuses on the comparison between HC and individuals with ASC. For the comparison between healthy controls themselves (HC vs HC), the group division involves creating two separate HC groups while maintaining the remaining stages of the analysis process.

3.4. Statistical Agnostic Mapping

SAM, or Statistical Agnostic Mapping [22], is a non-parametric ML method used for evaluating neuroimaging data at either the voxel or regional level. It addresses the issue of unstable risk estimates that arise from limited sample sizes by employing cross-validation (CV) techniques in ML. Moreover, SAM offers an alternative approach for mapping p -values that are corrected for FWE under *the worst case*, ensuring the reliability of inferential statistics for hypothesis testing. The methodology of SAM is grounded in the data and employs concentration inequalities to test opposing hypotheses or compare different models. SAM has been shown to be a highly competitive and complementary method to the SPM framework, which is widely accepted by the neuroimaging community. SAM generates activation maps similar to those obtained through voxel-wise analysis in SPM, but with a focus on regions of interest. It has been extensively developed and tested in scenarios characterized by a small sample-to-dimension

ratio and varying effect sizes, including large, small, and trivial effects.

3.4.1. Feature Extraction and Selection

The SAM procedure can be summarized into several steps as follows:

1. The data will be prepared by designing a comparison between groups, referred to as the design matrix. ROI will be selected for analysis, focusing on specific areas within the subjects' brains.
2. For each ROI, a feature extraction and selection stage will be conducted to derive the feature space. This involves identifying relevant features that contribute to the classification task. A SVM will be trained using Empirical Risk Minimization (ERM) to estimate the replacement error.
3. The empirical error or precision will be calculated based on the trained SVM model. Additionally, the true precision will be determined in the worst-case scenario with a probability of $1 - \delta$. This step helps assess the accuracy and reliability of the results.
4. The z -test statistic will be computed for each true precision to evaluate their significance. This statistical test assesses whether the observed results deviate significantly from what would be expected by chance, providing insights into the meaningfulness of the findings.

These steps collectively form the SAM procedure, allowing for the identification and evaluation of significant differences between groups in the selected regions of interest. In this study, default values are used for the SAM implementation (v1.0 [53]). The input data for SAM will consist of images divided into two classes, namely HC class images vs. ASC class images; and HC class images vs. HC class images. To select relevant features, we will employ a t -test. Within each ROI, SAM will calculate the t -statistic value for each voxel, and we will select the 50 voxels (features) with the highest t -values. This threshold of 50 voxels has been determined based on the consideration of images with a voxel size of 2x2x2 mm and an atlas comprising 116 regions, as it has consistently yielded favorable outcomes in previous studies[22]. Partial Least

Squares Regression (PLS) will be used for feature extraction[31], with a single PLS dimension being employed (see Appendix A.2). PLS has demonstrated its effectiveness in capturing relationships between brain activity and experimental design or behavioral measures within a multivariate framework. The complete analysis pipeline, which incorporates Feature Extraction and Selection (FES), is illustrated in Figure 2 as a block diagram.

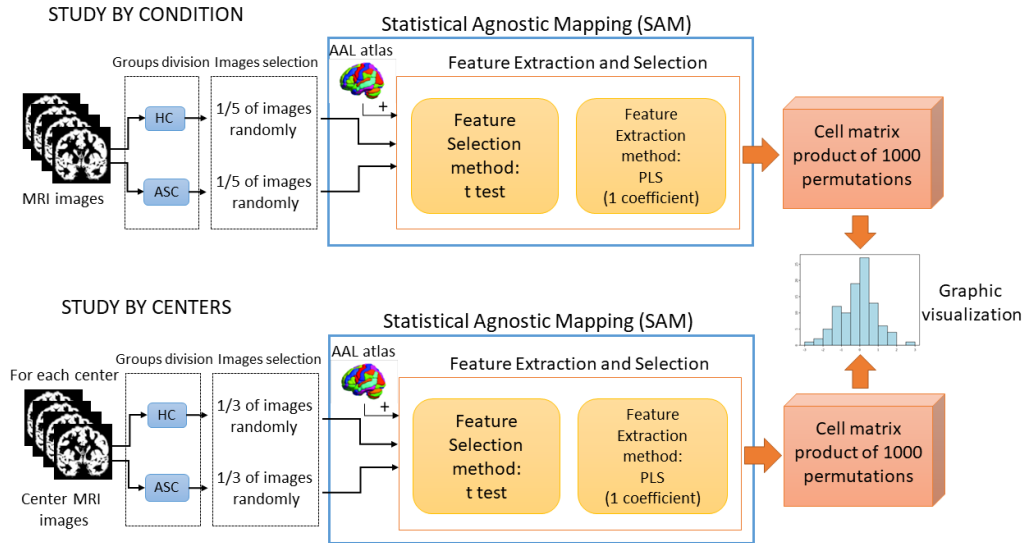


Figure 2: The block diagram illustrates the MRI analysis process incorporating SAM and the feature extraction and selection stage. Specifically, the diagram represents the comparison between HC and individuals with ASC. As for the comparison between HC themselves (HC vs HC), the group division will involve creating two separate HC groups, while retaining the remaining stages of the analysis process.

3.5. Statistical Analysis by permutation testing

In this article, we employ a two-sample statistical analysis using permutation tests [44, 20] to identify brain regions that exhibit statistically significant differences. The p -value will be calculated using equation (1), where the numerator represents the number of instances where the permutation test statistic \mathcal{T} exceeds the true precision, divided by the total number of permutations conducted. Adding 1 to both the numerator and denominator ensures the inclusion

of a fixed statistical value, thereby ensuring the validity of the test.

$$p\text{-value} = \frac{[\#\mathcal{T}_\pi \geq \mathcal{T}] + 1}{M + 1} \quad (1)$$

where M is the number of permutations.

The study involves analyzing brain images using two different approaches: by center and by condition. In each case, two types of comparisons will be conducted: between individuals with autism and controls (HC vs ASC), and between controls themselves (HC vs HC). When analyzing by center, these comparisons will be performed individually for each center. The purpose of conducting the study by center and by condition is to minimize the possibility of obtaining FP results caused by external factors unrelated to the disorder, such as variations in the instruments used to obtain the images, data acquisition processes, or other confounding factors. The comparisons of primary importance are those between HC and ASC, as they involve distinct classes of individuals and determine the presence of significant differences between the groups. However, the comparison of HC vs HC is included to identify any regions that may exhibit significant differences unrelated to the disorder, possibly due to chance or other external factors. If such regions emerge in both the HC vs HC and HC vs ASC comparisons, they can be disregarded as unrelated to the disorder.

To conduct the aforementioned comparisons, a permutation test will be employed, with $M = 1000$ permutations performed for each case[?]. The permutation test is a statistical significance test used to examine differences between groups. It involves calculating the statistic value for all possible rearrangements of observations within the different groups. In each permutation, the brain images will be divided into two groups of equal sizes: HC and individuals with ASC, or two HC groups.

3.6. Sample size and power calculations

A specific number of images will be randomly selected from each group for the analysis, assuming the sample size needed to detect the minimum detectable

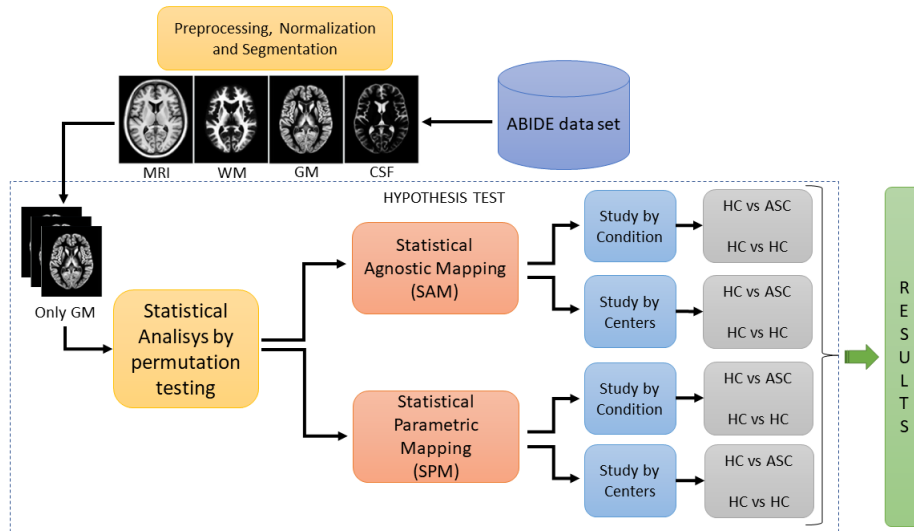


Figure 3: Block diagram about structure of the Autism Brain Imaging Data Exchange I (ABIDE I) dataset analysis.

effect. In the case of the study based on the condition of the patients (HC vs ASC), approximately 1/5 of the total number of images contributed by each group will be taken, resulting in 100 images from each group. Conversely, for the study conducted by centers, 1/3 of the images from each group will be selected individually at each center. This ensures a balance between the sample size and the available dataset, creating distinct subgroups in each permutation. The varying sample sizes are a result of the total number of samples available in each case, with the study by centers having a smaller number of available images. In each permutation, the selected images will be compared to one another using the respective mapping method being employed. This involves region-to-region comparisons using SAM and voxel-level comparisons using SPM. Figure 3 illustrates the framework of the analysis process.

4. Experimental results

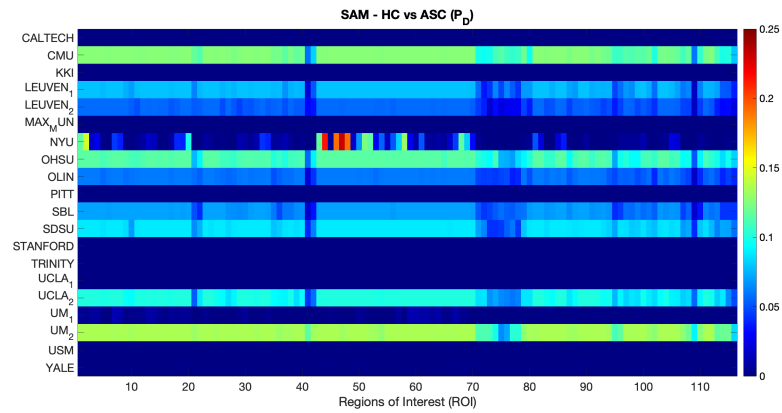
The initial analysis of the data will be conducted using the data-driven SAM method. The objective is to take advantage of the excellent control over FPs

provided by this method, in contrast to the optimistic clusterwise inference of parametric methods [16].

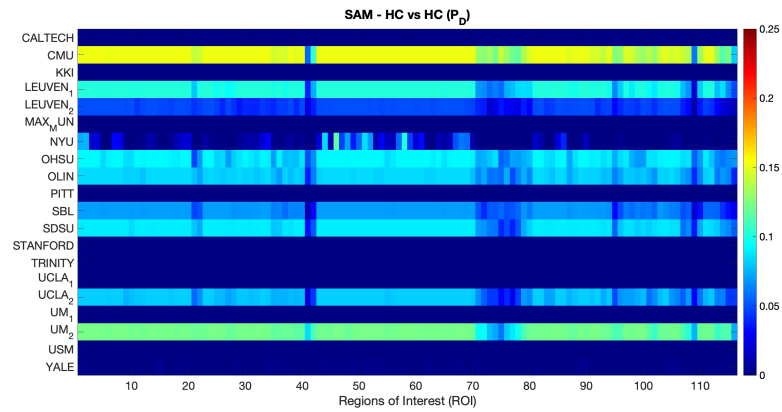
4.1. SAM analysis

Firstly, the analysis will be carried out based on the condition, where all the images contributed by each center will be grouped together, distinguishing between ASC and HC. With 1000 permutations and a probability of at least $1 - \alpha$ set at 0.95, we would expect around 50 FPs by chance under the null hypothesis. Therefore, regions that exhibit a number of significant differences exceeding 50 will be deemed significant (TP), as they fall within the predetermined 95% confidence level ($1 - \alpha$) in HC vs. ASC comparison. In the results obtained it can discern the presence of numerous regions displaying a notable number of significant differences. Surprisingly, even in the HC vs HC comparison, where any significant difference should be considered as a FP, regions exhibiting substantial differences are observed. Notably, both comparisons reveal the same significant regions with highly similar values, indicating that many of these differences are not solely attributable to the patient’s condition (if any) but rather to other factors. Consequently, in order to investigate whether any of these differences may be attributed to the distinct imaging centers contributing the data, a subsequent study will be conducted focusing on the centers.

The permutation test, along with SAM, is performed individually for each center in both comparisons (see figure 4 where we display “probability of detection”). Analyzing the results shown in the aforementioned figure, it is possible to distinguish three different sets of centers that show similar behaviour: (i) Firstly, there are centers where no significant differences are observed in any region, regardless of the comparison being made. While this outcome may be anticipated, as it suggests that no specific brain region distinguishes individuals with ASC from HC, it could be surprising that none of the regions exhibit even minimal differences across multiple brains, even if these differences are attributable to random factors. (ii) Secondly, there are centers where the HC vs HC comparison yields no significant differences in any region, similar to the previous case.



(a) HC vs ASC permutations comparison of each center with SAM



(b) HC vs HC permutations comparison of each center with SAM

Figure 4: Estimated probability of detection through permutation testing using the SAM mapping method. Each colormap rectangle represents one of the 116 brain regions defined in Table 2 of [57]. The color map depicts the probability of detection of significant differences observed in the regions during the permutation test.

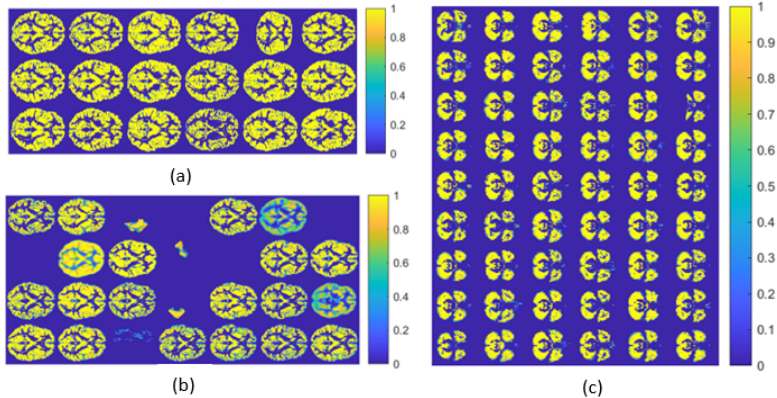


Figure 5: Brain mosaics from different centers to assess the presence of defective images. Specifically, the mosaics of three centers with distinct issues in their images are shown:(a) CALTECH’s cerebral mosaic, (b) YALE’s cerebral mosaic and (c) UM_1’s cerebral mosaic.

However, in the HC vs ASC comparison, almost all regions demonstrated significant differences, with remarkably similar frequencies. This is an exceptionally unusual scenario, as it is highly unlikely for all brain regions to exhibit such consistent and significant differences. (iii) Lastly, the centers NYU, UM_1, and YALE exhibit more expected results. In both comparisons, these centers show a mixture of regions with significant differences and regions without significant differences. Overall, these findings highlight the variability in results across centers, with some centers showing no significant differences (conservative behavior of the test), others displaying abnormal patterns of significant differences (nuisance effects), and a few demonstrating more “typical outcomes” with a mix of significant and non-significant regions in *both comparisons*.

The initial analysis was performed without accounting for the presence of poor quality images, as shown in Figure 5. Their presence can be attributed to errors in the acquisition or pre-processing pipeline, and affects every group randomly. Therefore, the balance in age or center is not affected by excluding them. The impact of incorporating defective images in the region detection process can be assessed by subsequently removing them from the dataset, thereby assessing the overall influence of noisy data.

4.1.1. An analysis removing outliers

By visual inspection, 21 images with defects that made them unusable were detected and discarded. After conducting subsequent analyses excluding the aforementioned images, it was found that the new results were highly consistent with the previous findings. However, there were notable changes in certain centers. The centers belonging to the second case described earlier now exhibited results where all regions displayed significant differences in both the HC vs ASC and HC vs HC comparisons. Additionally, the NYU center showed variations in the significance levels across different regions. On the other hand, the UM_1 center fell into the second case category, showing no effect results in the HC vs HC comparison and only minor differences in the HC vs ASC comparison, which were not significant as they fell below the threshold of 0.05. Similar to UM_1, the YALE center could also be classified as the second case, as it exhibited various regions with a similar number of differences in both comparisons. However, like UM_1, none of the regions in the YALE center demonstrated significant differences that surpassed the threshold for significance.

Figure 4 provides a summarized visualization of the probability of detection P_D of significant differences observed in each center, represented by a color map. After eliminating the defective scans, certain centers show a lack of significant differences across all brain regions (falling into the first case described earlier). Conversely, centers exhibiting a constant P_D across different regions belong to the second case discussed previously. Among the centers, the NYU center stands out as its results align more closely with the expected outcomes and are similar to those obtained when studying patients according to their condition. It is worth noting that some specific centers display high P_D , i.e. >0.05 in almost all regions. The high frequency of significant differences observed corresponds to very limited sample sizes, with sizes smaller than 17 scans, in relation to the 'magical' number proposed in [19].

Moreover, a new permutation test was conducted to study all the subjects according to their condition. The results, as shown in Figure 6, indicate that the

regions exhibiting significant differences remain largely consistent in both comparisons. However, the frequency of these differences slightly changed after the elimination of the defective scans. Notably, regions such as Postcentral_R and Occipital_Mid_L have emerged as significant in the updated results, as shown in Figure 7.

Figure 8 illustrates the observed difference in P_D between the analysis conducted with the inclusion of defective scans and the analysis performed without them. This can be employed to assess the impact of noisy data on the detection of significant differences between study groups.

Based on the results obtained from the analysis by centers, we can conclude that centers characterized by a limited number of patients do not possess a sufficient sample size to yield meaningful and reliable insights. These centers provide overly optimistic or pessimistic maps of significance as shown in figure 4. In the case of the NYU center, where a substantial number of patients are available, it presents an opportunity for further in-depth study, offering the potential to generate more robust and informative outcomes.

4.1.2. Study of NYU Center

The NYU center, with its large number of images, provides a robust dataset for focused studies. However, the results obtained from the permutation test in the NYU center reveal that the same brain regions consistently exhibit significant differences in both comparisons, while other regions consistently show no significant differences (Figure 9). Notably, posterior brain regions such as Calcarine_R, Cuneus_R, Lingual_L, and Lingual_R stand out prominently.

Considering the smooth changes in frequencies observed across different centers in figure 4, it is plausible that a relationship exists between the size or number of voxels comprising each region and its significance. On the left in Figure 9c, we show a scatter plot comparing the voxel size of each region with the number of times it exhibits significant differences (statistical power if we assume an effect in the sample). A threshold of 0.05 has been set on the y-axis (significance level). The scatter plot suggests a relationship between these two

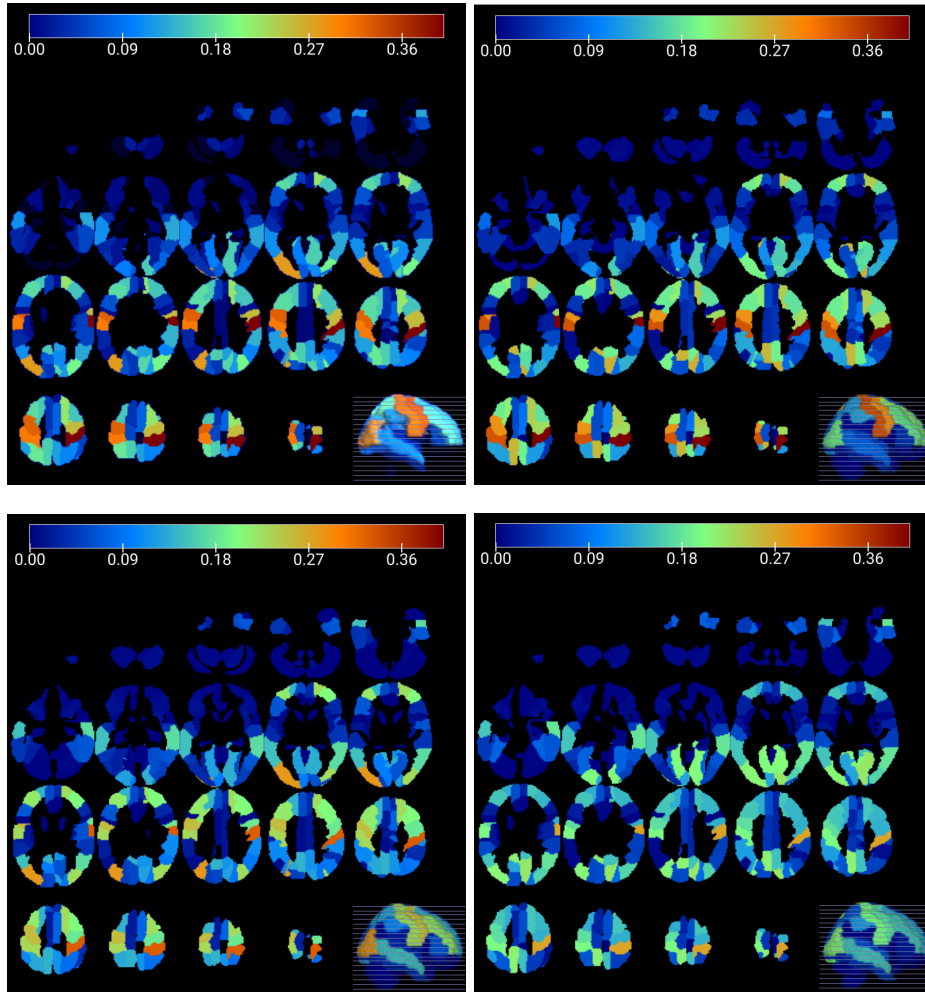


Figure 6: All center study using the SAM mapping method, highlighting the P_D observed in each region during the comparisons HC vs ASC and HC vs HC from left to right, respectively. Above are the comparisons prior to the removal of flawed scans. Below, the same comparisons are presented after removing flawed scans.

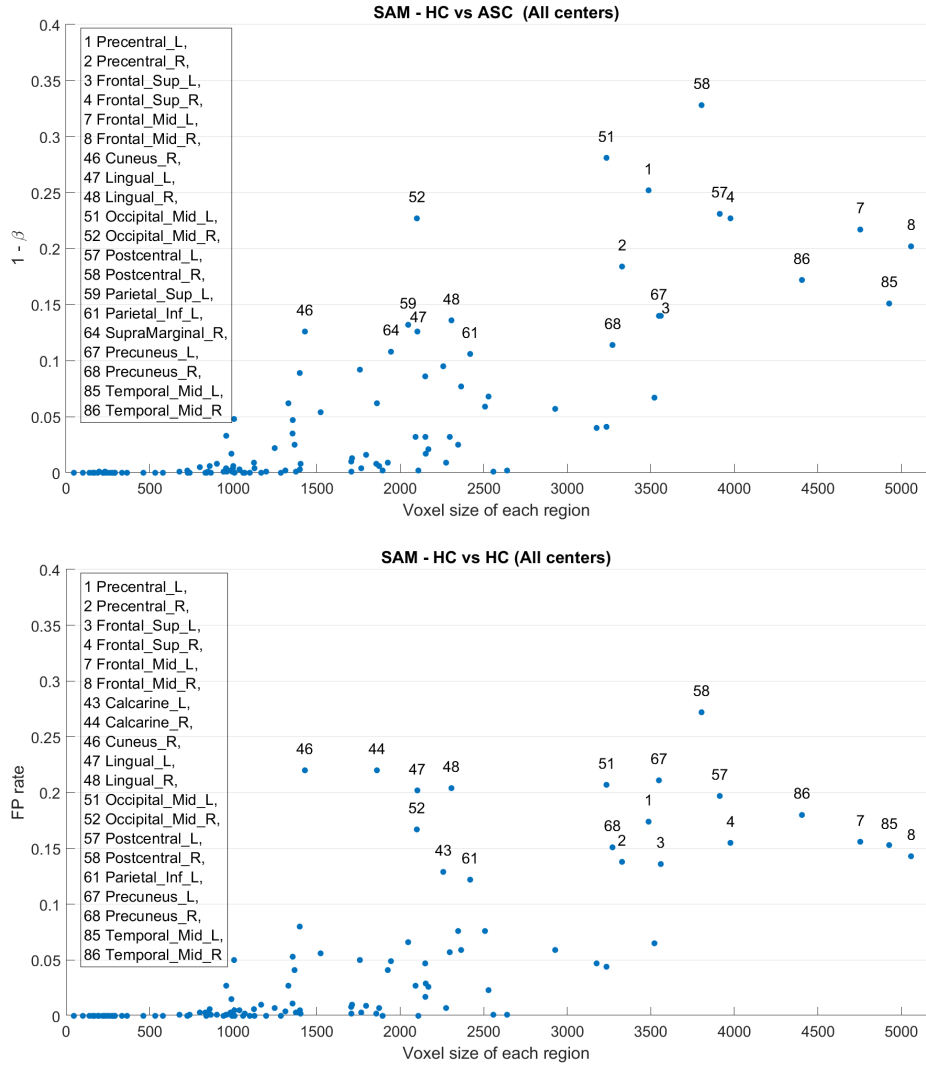


Figure 7: Upper image shows estimated P_D using SAM mapping method during the all centers comparison. Lower image shows FP rate in the same conditions. Each data point on the diagram represents a specific brain region, highlighting the most prominent ones.

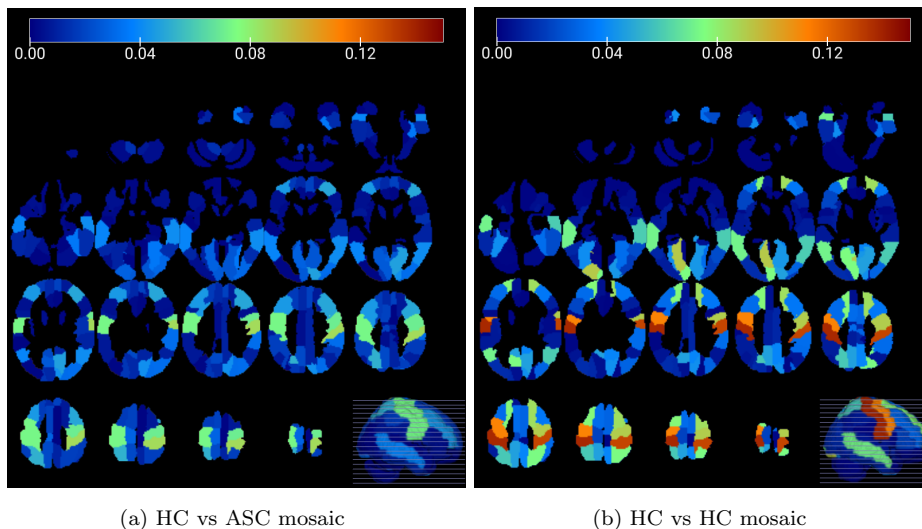
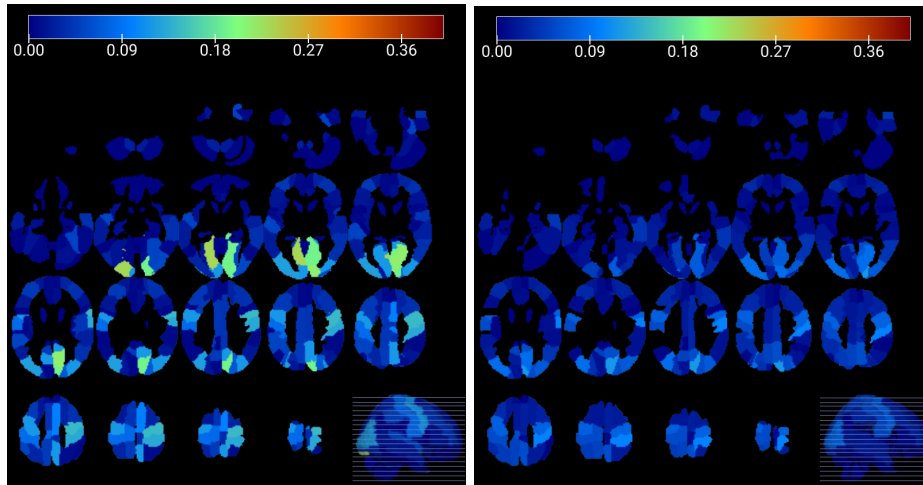


Figure 8: Differences between the P_D at each brain region including or excluding noisy data for HC vs ASC and HC vs HC comparisons.

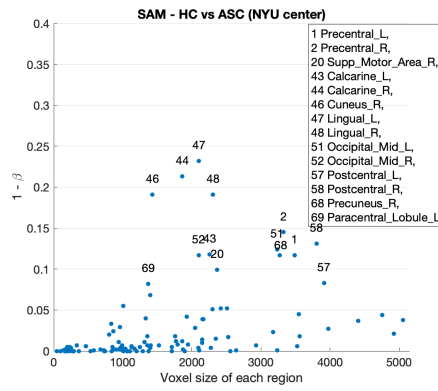
variables, indicating that the power of the test increases as larger regions are considered. It can be inferred that regions below 1000 voxels are never significant. These findings could highlight the importance of considering multivariate approaches and the size of brain regions when analyzing significance, as larger regions provide more reliable and informative results in neuroimaging studies.

Unfortunately, a similar effect on the rate of false positives (FPs) is observed in the right part of the same figure (Figure 9d). This observation indicates that there is indeed a trivial effect present in the entire dataset, with effects correlated in both groups. Upon closer examination of the results from the permutations test, it becomes apparent that the brain region with the most significant differences in both comparisons occurs approximately 240 times out of the 1000 permutations. The calculated p -values (average) for the brain regions in Table 2 were found to be higher than the predefined significance level of $\alpha = 0.05$ (see Table 2). Therefore, besides the abnormal rate of FPs, it can be concluded that similar brain regions in the NYU center images exhibited non-significant differences in both comparisons. However, the surprisingly high

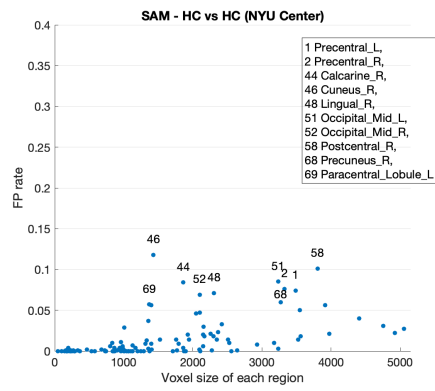


(a) HC vs ASC NYU

(b) HC vs HC NYU



(c)



(d)

Figure 9: Brain regions with significant differences in both comparisons (a) HC vs ASC and (b) HC vs HC using the SAM permutation test after defective images removal in NYU. (c) Region voxel size vs. estimated P_D in the HC vs ASC comparison using SAM. (d) Region voxel size vs. FP rate in the HC vs HC comparison using SAM. Each data point on the diagram represents a specific brain region, highlighting the most prominent ones.

rate of FPs in the HC vs. HC comparison affects the computation of p -values in the ASC vs. HC study, as shown at the bottom of the table. Assuming the p -values follow a normal distribution according to the empirical rule (68-95-99.7), the lack of evidence for rejecting the alternative hypothesis doesn't prove that the effect does not exist at the significance level (95%).

4.2. Analysis with SPM

The initial study was conducted by grouping all the images based on patient condition, disregarding the centers to which they belong. The images were divided into two groups: ASC and HC. Two variables were studied: the frequency at which different voxels were present in each region during the 1000 permutations, and the number of significant voxels in each region. These two measures account for the significance of a region.

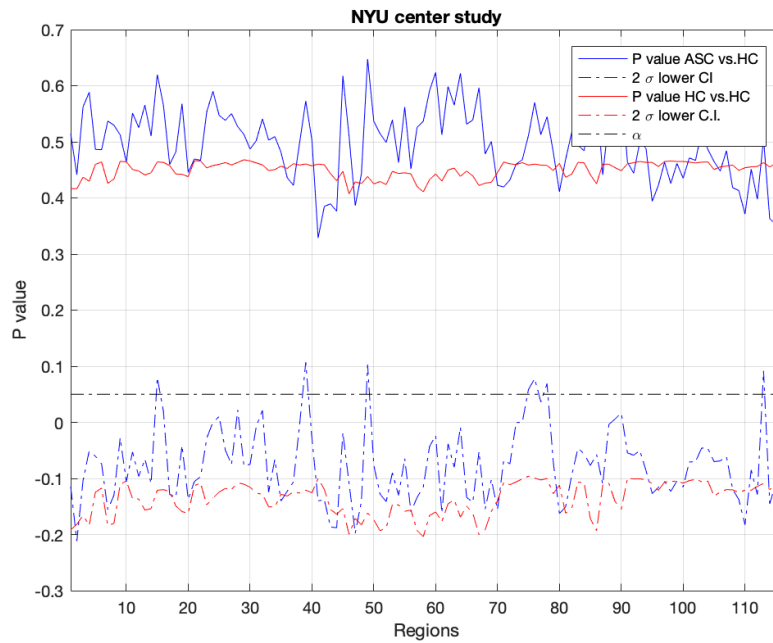
At the bottom of Figure 10, we computed the P_D of the SPM voxelwise statistical framework and compared it to the one obtained with the SAM method. As clearly shown in the figure, SPM did not provide the nominal value of 0.05, indicating an overly super-conservative method. This behaviour is indeed persistent in the studies with larger samples sizes as shown in the next section. Following these results, the p -value analyses did not reveal any evidence to reject the null hypothesis at the significance level.

4.2.1. Study by center

The SPM analysis failed in Group I (CALTECH, KKI, LEUVEN 1, LEUVEN 2, MAX MUN, OLIN, SBL, SDSU, STADFORD, TRINITY, USM) centers due to a limited number of samples available for analysis. On the other hand, the NYU center, which has the largest number of images, demonstrates minimal voxels with differences and a significantly lower frequency of regions showing significant differences. In fact, the regions exhibiting differences in the NYU center fall well below the threshold of 50, which was previously established as the nominal value or the expected value of FPs under the null hypothesis.

Table 2: P-values calculated for the regions of the NYU center. Only the regions that exhibited a frequency of significant differences within the confidence interval are included.

Regions	p -value	Regions	p -value
Precentral_L	0.3337	Occipital_Mid_R	0.3566
Precentral_R	0.4096	Occipital_Inf_R	0.4216
Supp_Motor_R	0.4296	Fusiform_R	0.4316
Calcarine_L	0.4945	Postcentral_L	0.3177
Calcarine_R	0.4705	Postcentral_R	0.3037
Cuneus_R	0.3317	Parietal_Inf_L	0.3656
Lingual_L	0.4575	Precuneus_L	0.2757
Lingual_R	0.4146	Precuneus_R	0.3776
Occipital_Sup_R	0.3347	Paracentral_Lob_L	0.3576
Occipital_Mid_L	0.3487	Temporal_Sup_L	0.4046



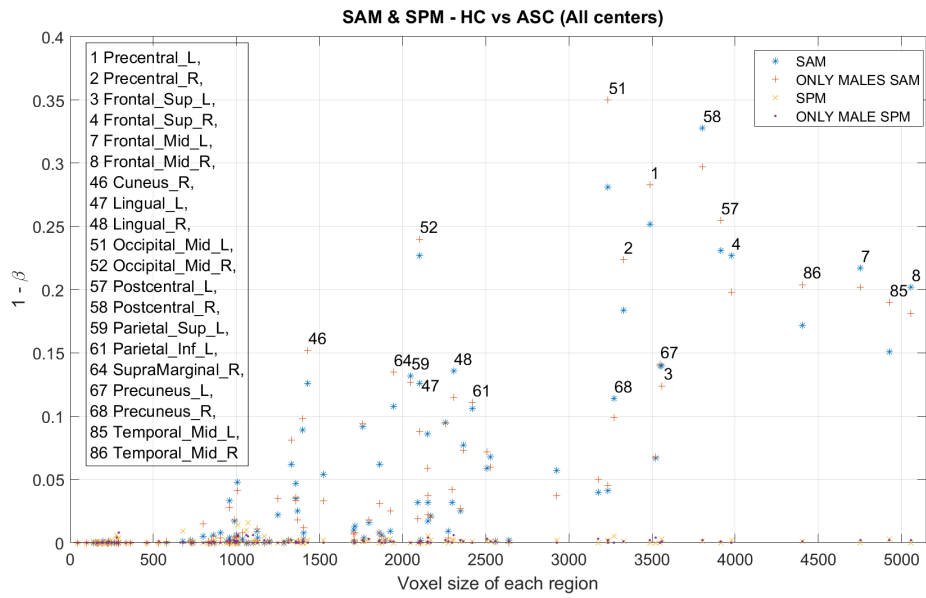
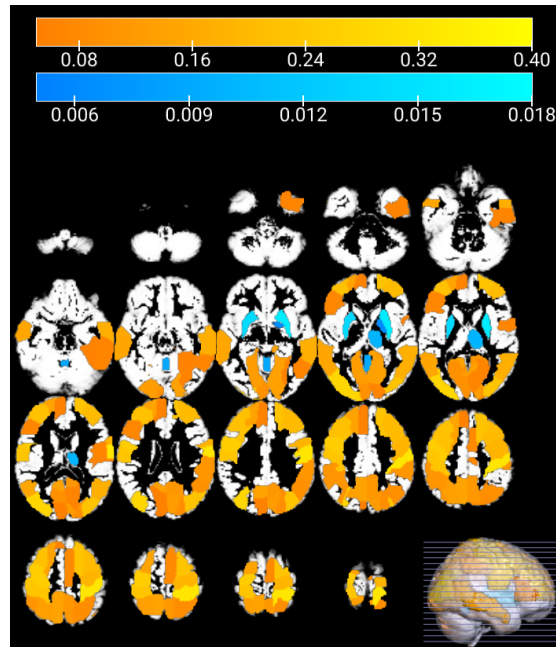


Figure 10: SAM and SPM results for HC vs ASC all centers comparison. In the upper image, it is represented in orange the P_D at each brain region detected by SAM statistical method and in blue the P_D detected by SPM. In the lower image, the SAM and SPM comparison is presented, including their respective analyses with male subjects only.

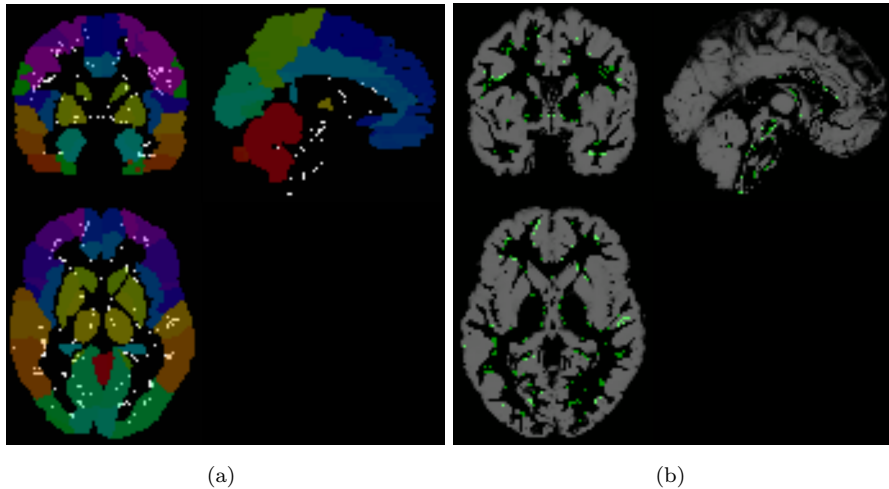


Figure 11: SPM t-map in ASC vs HC comparison of OLIN center, compared to the AAL atlas (a), and compared to the GM map (b).

This observation holds true for both the study by condition and the study by centers using SPM.

On the contrary, some limited samples exhibit a higher number of voxels showing differences after the contrast analysis. This is clearly an undesirable behaviour taking into account the outcome with larger sample sizes. Taking the OLIN center as an example, we can observe the voxels that have been identified as different after the permutation test using SPM in Figure 11, superimposed on the image provided by the AAL atlas. These voxels, located near the edges of different regions, can be attributed to registration artifacts, which can arise from anatomical variations among subjects or discrepancies between the atlas-defined regions and the detected regions during image registration. Also, some differences are concentrated in the brain stem, as it is shown in the same figure.

Figure 12 reveals the frequency of significant voxels across various brain regions following the SPM contrast for centers with limited sample sizes (Group I). Notably, these centers exhibit relatively high voxel frequencies and disparities between regions, along with numerous algorithmic issues during the analysis.

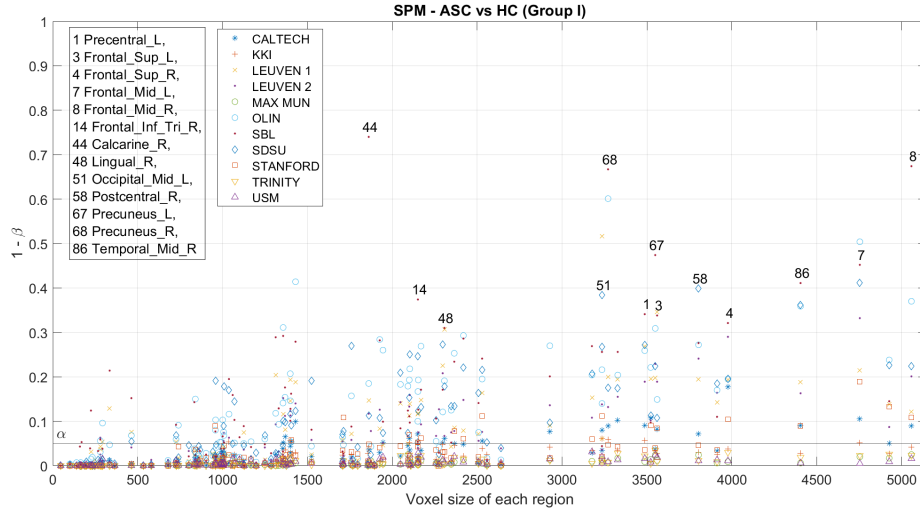
Consequently, it can be concluded that the large number of voxels detected in these centers is not attributable to the identification of a specific region marking differences between individuals with autism and healthy controls. Instead, it likely stems from center-specific characteristics, such as sample realization, confounding effects, etc.

Figure 13 show the results on centers larger sample sizes (Group II: NYU, PITT, UCLA_1, UM_1, and YALE). Although there are regions that exhibit a substantial number of voxels, these completely vanish in the analysis across all centers.

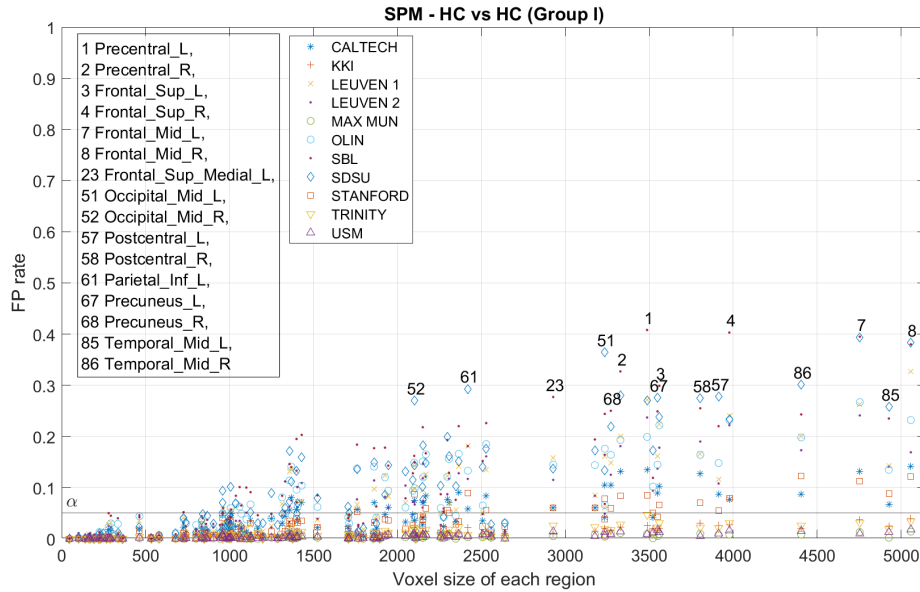
After analyzing the images with SPM, both by condition and by center, it can be concluded that SPM does not identify any region or voxel that exhibits statistically significant differences at $\alpha = 0.05$. Therefore, based on the results obtained, it could be inferred that there are no specific brain regions or voxels that can be considered reliable indicators for distinguishing between individuals with autism and neurotypical individuals. Taking into account all the issues and artifacts found in the analyzed datasets, this is rather a consequence of the super conservative behavior of voxelwise statistical inferences in the SPM method.

5. Discussion

Throughout this discussion, the results ascertained from performing image analysis on the ABIDE I database using each of the selected mapping methods will be scrutinized to determine the extent of their resemblance or divergence. Emphasis will be placed on two key aspects: (1) the study encompassing patient conditions, and (2) the examination of individual centers within the ABIDE I database, accounting for their respective images. Subsequently, a comparative analysis will be conducted to juxtapose our findings with the existing body of scientific literature. This examination aims to assess the extent of concurrence between our results and the previously documented research in the field.

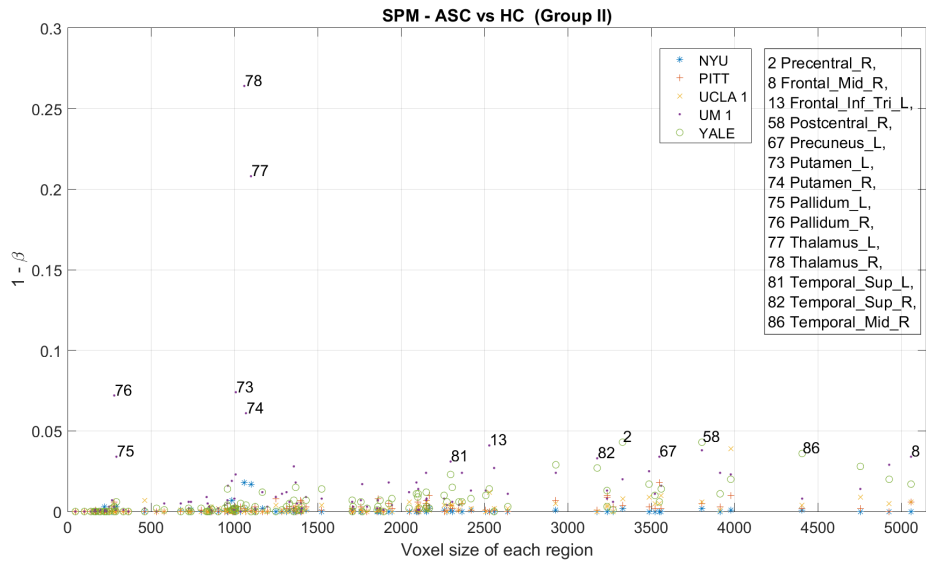


(a) ASC vs HC voxels comparison of Group I centers with SPM

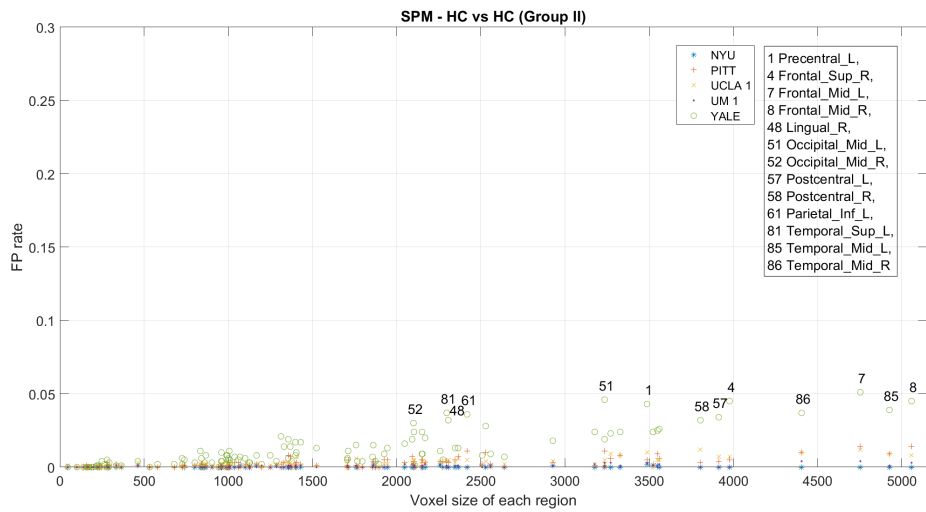


(b) HC vs HC voxels comparison of Group I centers with SPM

Figure 12: Estimated P_D (upper) and FP rate (lower) with SPM during the Group I centers analysis. Each point on the diagram represents a specific brain region, highlighting the most prominent ones.



(a) ASC vs HC voxels comparison of Group II centers with SPM



(b) HC vs HC voxels comparison of Group II centers with SPM

Figure 13: Estimated P_D (upper) and FP rate (lower) with SPM during the Group II centers analysis. Each point on the diagram represents a specific brain region, highlighting the most prominent ones.

5.0.1. SAM and small sample sizes

After analyzing each center using SAM, it was observed that some centers had completely null results, meaning that their regions did not exhibit any significant differences during the 1000 permutations, not even due to randomness. Conversely, there were centers that showed regions with consistently similar levels of significance across the 1000 permutations, illustrated in Figure 4.

The primary reason for these results can be attributed to the insufficient number of samples available at each center, which provides us with a super-conservative upper bound. Most centers had relatively small databases, with fewer than 20 samples for each group, except for a few centers. Additionally, the removal of defective brain images further decreased the sample size. Consequently, during the permutation test, the total number of samples ranged from 8 to 20, evenly distributed between the two groups. Such a limited sample size could strongly influence the atypical results observed in these cases, as SAM assumes some degree of uncertainty in the data and applies statistical corrections based on the assumption of randomness.

Moreover, the presence of artifacts and confounding effects in the sample realization provides “actual” classes and subclusters in the population, resulting in heterogeneous samples. Consequently, with a small number of samples, null empirical errors can be reached, compensating for the ultra-conservative upper bounds, even in low-dimensional scenarios. Therefore, SAM’s methodology only reflects the actual classes that conform to the groups.

Considering previous studies indicating brain differences related to sex within the autism spectrum[23], the differentiation of male subjects from female subjects was studied. Focusing solely on male patients due to their larger representation in the dataset, the results obtained did not deviate from previous findings, suggesting that the sex of the patient did not significantly influence the outcomes, as shown in Figure 10b. This lack of impact could be attributed to the small proportion of female patients in the dataset, limiting their statistical relevance.

5.1. Study by condition

SAM analysis revealed the presence of brain regions with a notable number of significant differences for both comparisons (HC vs ASC and HC vs HC), even after excluding defective brains. However, the observed differences did not reach a sufficiently high level compared to the number of permutations conducted, thereby precluding the identification of any decisive regions as shown in the p -value analysis. Indeed, upon fixing the significance level and calculating the p -value for each region, it was determined that none of them exhibited statistically significant differences, although in this case we prefer to claim that there is no sufficient evidence in support of the alternative hypothesis. Similarly, the analysis performed with SPM demonstrated a scarcity of significant voxels in the T-maps. The frequency of regions exhibiting differences at voxel level during the 1000 permutations was even below the nominal level (50), affirming the absence of statistically significant differences in any particular region using this over-conservative method.

Figure 10 provides a comparison of SAM and SPM results, visualizing regions identified as different by SAM along with their corresponding frequency values using an orange color map, and highlighting the number of voxels that manifested differences after the SPM contrast using a blue color map. SAM highlights regions as Postcentral_R, Postcentral_L, Occipital_Mid_L, Occipital_Mid_R, Precentral_L, among others. Meanwhile, SPM highlights regions as Putamen_L, Putamen_R, Thalamus_R, Vermis_4.5, among others. Notably, the highest concentration of voxels detected by SPM was observed in regions where SAM indicated no or minimal differences, while regions exhibiting more significant differences according to SAM showed scarce significant voxels. Consequently, both methods did not individually establish statistically significant differences but contradicted each other in identifying regions with great disparities.

5.2. Study by acquisition sites

Both SAM and SPM methods revealed the need to differentiate the NYU center from the remaining centers in the study. In both methods, some centers have regions with significantly higher frequency or voxel count compared to NYU or the study conducted based on the subjects' condition. However, it is highly likely that these results, particularly in SAM where the values among centers were similar, stem from the limited number of images available for each center. The limited number of images, regardless of the mapping method employed, contributes to errors that compromise the reliability of the obtained results. Conversely, when the images from all centers are aggregated and analyzed as a whole (study by condition), the differences found between groups dilutes.

Regarding the NYU center, both SAM and SPM mapping methods exhibit remarkably similar results compared to the results obtained from the study conducted based on the subjects' condition. This can be attributed to the fact that NYU contributes the largest number of samples, making it the most suitable center for in-depth examination among the 20 centers comprising the ABIDE I database.

In SAM, the NYU center demonstrates numerous brain regions that exhibit differences exceeding 100 occurrences during the 1000 permutations. Notably, during the HC vs ASC comparison, which is of particular interest, the regions Calcarine_R, Cuneus_R, Lingual_L, and Lingual_R emerge as the regions with the most significant differences, with two of them exceeding 200 out of 1000 occurrences. However, SPM analysis reveals a minimal number of voxels with differences after the contrast in the NYU center. The regions Hippocampus_R, Thalamus_L, and Thalamus_R exhibit the highest concentration of these differing voxels, while SAM either indicates no differences or minimal distinctions in these areas. Consequently, it can be concluded that both mapping methods contradict each other by identifying entirely distinct regions as positive. Nevertheless, both approaches reach the same statistical conclusion from the analysis of p -values.

Figure 14 visually presents the comparison between SAM and SPM results,

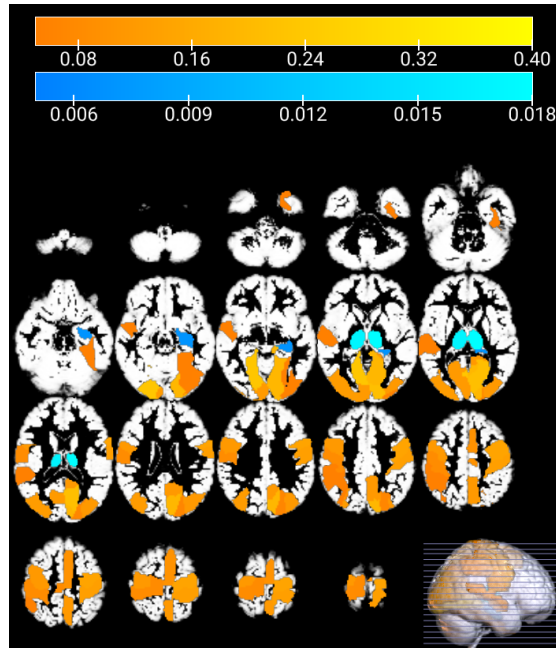


Figure 14: Comparison of SAM and SPM results for HC vs ASC comparison at NYU center. In orange, the differences in brain regions detected by SAM statistical method. In blue, the differences detected by SPM.

illustrating the regions identified by SAM as having significant differences along with their corresponding frequency denoted by an orange color map, as well as the most significant voxels detected by SPM, denoted by a blue color map.

This finding provides evidence that the examination of centers does not reveal any regions or voxels that exhibit statistically significant differences between individuals with ASC and healthy controls. The absence of significant findings can be attributed to two factors: firstly, the limited availability of samples in the majority of centers, which compromises the statistical power of the analysis; and secondly, the regions under investigation do not demonstrate a substantial number of differences relative to the permutations conducted. Additionally, it is noteworthy that each statistical method identifies disparate regions as significant, despite employing the same set of images.

5.3. Final remarks on the ABIDE dataset

The findings from the analysis of ABIDE I database images based on the subjects' condition indicate the absence of any specific brain region that can be deemed crucial in distinguishing individuals with ASC from healthy controls. The lack of statistically significant differences suggests that a comprehensive differentiation between the two groups cannot be achieved solely through this approach.

One possible explanation for these outcomes is the amalgamation of images from various centers within the ABIDE I database, resulting in a heterogeneous multicenter database. Autism is inherently characterized by its heterogeneity, encompassing diverse symptoms and characteristics, hence its classification as a spectrum disorder [35, 38, 58]. Consequently, attempting to study such a complex disorder using a database that comprises multiple centers with distinct imaging protocols, equipment, and laboratory settings, among other variables, may yield inconsistent results[?]. To address this, the utilization of larger databases characterized by uniformity in scanner type and imaging procedures would be advantageous. By ensuring uniformity and control over extraneous factors unrelated to the disorder, the potential for false results arising from these confounding influences can be minimized. Therefore, it is advisable to avoid pursuing a multicenter approach in neuroimaging research when studying disorders as heterogeneous as autism without carefully controlling confounding variables, sample size, imaging protocols and other sources of variability not related to the disease.

5.4. Comparison with the extant literature

Currently, numerous studies have investigated the application of deep learning techniques using the ABIDE I database to classify autism, wherein they have identified specific brain regions that exhibit notable correlations. These regions often manifest in the posterior section of the brain, including the Occipital Pole, Precuneus Cortex, Intracalcarine Cortex, Left Lingual Gyrus, and others [9, 24, 61, 42, 28, 17]. These areas hold potential significance in our

image comparison study. Focusing solely on the HC vs ASC comparison, the SAM analysis has revealed that the regions displaying a greater frequency of significant differences, both in the study based on the patients' condition and in the study conducted at the NYU center (yielding the most favorable outcomes), are predominantly located in the posterior regions of the brain. Noteworthy areas include Occipital_Mid_L, Calcarine_R, Cuneus_R, Lingual_L, Lingual_R, among others. Additionally, the Postcentral region stands out in the SAM analysis and in certain publications. Thus, these areas may align with those exhibiting robust correlations in previous studies. However, the SPM analysis reveals that the majority of differences, or areas with the highest voxel concentration after contrast, are situated in the central and inner regions of the brain. This pattern is observed both in the analysis based on the patients' condition and in the study encompassing centers that encountered no issues during the analysis. Noteworthy regions encompass Putamen_L, Putamen_R, Thalamus_L, Thalamus_R, Frontal_Sup_R, Temporal_Mid_R, among others. Figures 10 and 14 prominently depict the regions of interest identified by both mapping methods, providing a clear visual representation.

SAM, in contrast to SPM, produces results that exhibit greater resemblance to the findings reported in existing literature, indicating overlapping regions of significance within the brain. Although these results may not meet the threshold for statistical significance, they contribute to narrowing down the search for key brain regions that can reliably differentiate between individuals with autism and neurotypical individuals.

It is noteworthy that certain studies, such as [49, 30, 41], have reported classification accuracies exceeding 80% when utilizing images from the ABIDE I database, with some works estimating the classification performance of the proposed methods to 100%, as demonstrated in [55]. However, our present research indicates that achieving such a high level of accuracy in autism classification with the ABIDE I database is highly improbable, primarily because there is a lack of distinct structural brain patterns that can serve as clear differentiator between ASC and HC. The use of the ABIDE I database, as observed in this

study, does not yield to significant differences in structural brain patterns of heterogeneous disorders such as autism.

6. Conclusions

Throughout this study, our objective was to identify specific brain regions that could serve as reliable biomarkers in ASC, utilizing the diverse and multisite ABIDE I database. The images were analyzed by permutation tests and SAM and SPM, studying the influence of several factors, such as the presence of noisy images, determining differences by center or by condition. The results were not consistent, exhibiting those obtained with the SAM method, when compared to the SPM method, a much closer resemblance to the findings presented throughout the existing literature.

The main finding of the present analysis suggests that no significant differences can be observed in gray matter tissues of any specific brain region between individuals with ASC and HC subjects in structural MRI images of the ABIDE I database. This finding does not definitively dismiss the possibility of the existence of specific structural differences implicated in autism. However, it does suggest that the structural MRI data provided by the ABIDE I database, given its inherent heterogeneity, may not offer the best solution for investigating this phenomenon.

Acknowledgements

This work was supported by the MCIN/ AEI/10.13039/501100011033/ and FEDER “Una manera de hacer Europa” under the PID2022-137451OB-I00 project, by the Consejería de Economía, Innovación, Ciencia y Empleo (Junta de Andalucía) and FEDER under CV20-45250, A-TIC-080-UGR18, B-TIC-586-UGR20 and P20-00525 projects.

Appendix A.

Appendix A.1. Hypothesis tests

The study involves conducting a hypothesis test, where the null hypothesis (H_0) represents the accepted belief thus far, which assumes no brain differences between individuals with autism and those without autism. The alternative hypothesis (H_1), the contrast to the null hypothesis, suggests the presence of significant differences in the brains of autistic and non-autistic individuals.

The significance level α is set at the standard value of 0.05, indicating the threshold for determining statistical significance. During the statistical analysis of the brain images, if the probability or p -value of the obtained results for the different brain regions is found to be less than the predetermined significance level α (<0.05), it would indicate that the observed findings are highly unlikely to occur by chance alone. In such a case, the null hypothesis would be rejected, and it would be concluded that there are statistically significant brain differences.

Appendix A.2. Selection of PLS dimension

SAM employs a FES stage on each ROI within the images. In this study, the feature extraction method chosen is PLS, with the dimension set to 1. The selection of 1 as the dimension of PLS is based on the observation that increasing the number of coefficients or dimensions leads to less significant results, as depicted in Figures A.15 and A.16. These figures illustrate the HC vs ASC comparisons conducted on both the entire image dataset according to their condition (Figure A.15) and the individual dataset from the NYU center (Figure A.16). Only this comparison is presented since it is of utmost importance in this study, and the NYU center is highlighted due to its substantial individual sample size.

As the dimension of PLS increases, the frequency values of the brain regions generally decline, particularly in the case of the NYU center where this reduction is more pronounced. This implies that the utilization of a large number of PLS

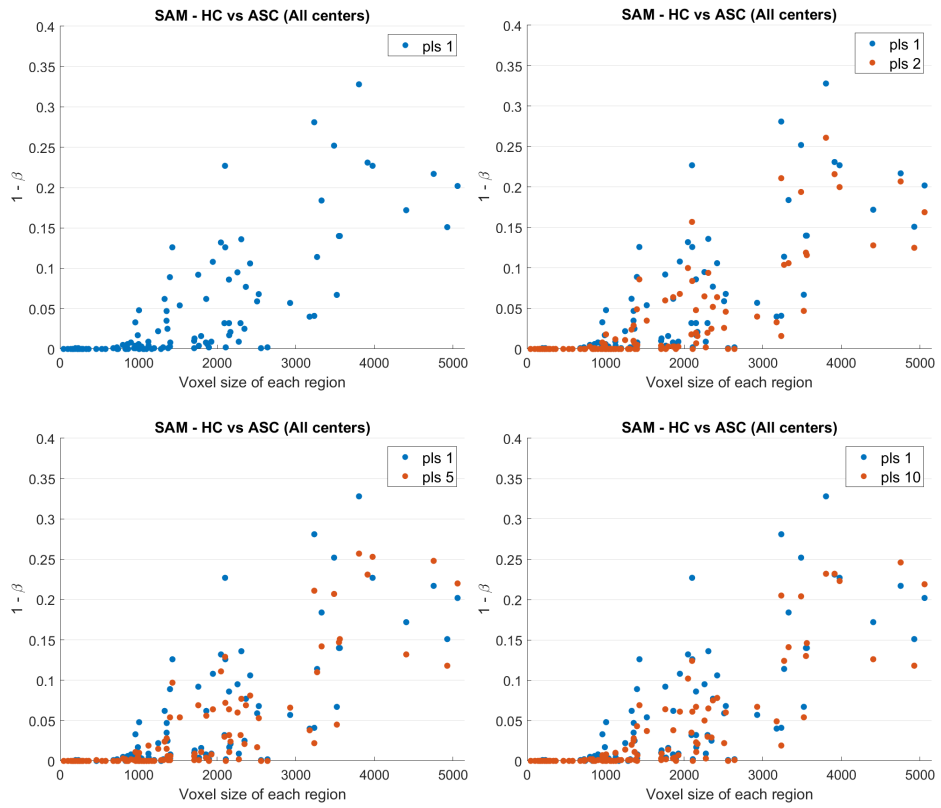


Figure A.15: Subplot on comparison between different values of dimensions for PLS as a method of feature extraction in SAM analysis for all centers HC vs ASC comparison.

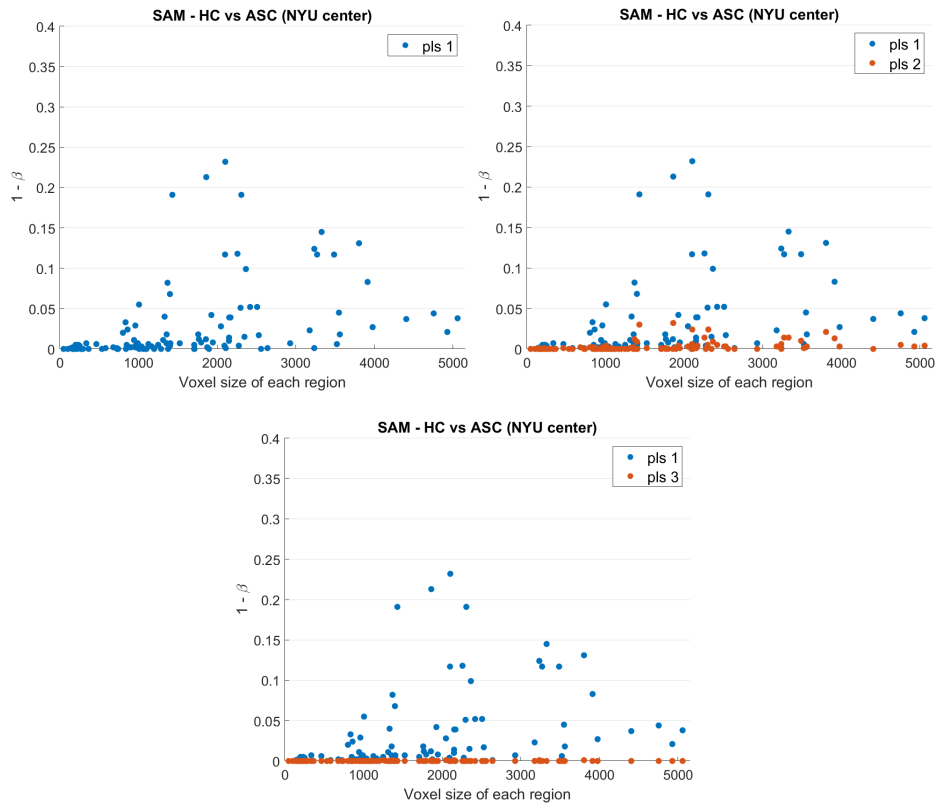


Figure A.16: Subplot on comparison between different values of dimensions for PLS as a method of feature extraction in SAM analysis for NYU center HC vs ASC comparison.

components poses a potential risk of overfitting in heterogeneous environments. This risk arises from the fact that PLS aims to maximize the fisher discriminant ratio (FDR) between the two groups analyzed. Consequently, as the number of PLS components increases, the selected features become more complex and adapted to the specific characteristics of the data. Therefore, the selection of 1 as the PLS dimension is the most suitable option for the analysis throughout this study.

References

- [1] *VBM8-Manual.pdf*. Available: <http://dbm.neuro.uni-jena.de/vbm8/VBM8-Manual.pdf>.
- [2] Mohamed T. Ali, Yaser ElNakieb, Ahmed Elnakib, Ahmed Shalaby, Ali Mahmoud, Mohammed Ghazal, Jawad Yousaf, Hadil Abu Khalifeh, Manuel Casanova, Gregory Barnes, and Ayman El-Baz. The Role of Structure MRI in Diagnosing Autism. *Diagnostics (Basel, Switzerland)*, 12(1):165, January 2022. ISSN 2075-4418. doi:10.3390/diagnostics12010165.
- [3] Rushil Anirudh and Jayaraman J. Thiagarajan. Bootstrapping Graph Convolutional Neural Networks for Autism Spectrum Disorder Classification, October 2018. URL <http://arxiv.org/abs/1704.07487>. arXiv:1704.07487 [cs, stat].
- [4] Devanshu Arya, Richard Olij, Deepak K. Gupta, Ahmed El Gazzar, Guido Wingen, Marcel Worrying, and Rajat Mani Thomas. Fusing Structural and Functional MRIs using Graph Convolutional Networks for Autism Classification. In *Proceedings of the Third Conference on Medical Imaging with Deep Learning*, pages 44–61. PMLR, September 2020. URL <https://proceedings.mlr.press/v121/arya20a.html>. ISSN: 2640-3498.
- [5] John Ashburner and Karl J. Friston. Voxel-Based Morphometry—The Methods. *NeuroImage*, 11(6):805–821, June 2000. ISSN 1053-8119.

doi:10.1006/ning.2000.0582. URL <https://www.sciencedirect.com/science/article/pii/S1053811900905822>.

- [6] American Psychiatric Association, editor. *Guía de consulta de los criterios diagnósticos del DSM-5*. American Psychiatric Publishing, Arlington, VA, 2014. ISBN 978-0-89042-551-0.
- [7] E. H. Aylward, N. J. Minshew, K. Field, B. F. Sparks, and N. Singh. Effects of age on brain volume and head circumference in autism. *Neurology*, 59(2):175–183, July 2002. ISSN 0028-3878. doi:10.1212/wnl.59.2.175.
- [8] Carl C. Bell. DSM-IV: Diagnostic and Statistical Manual of Mental Disorders. *JAMA*, 272(10):828–829, September 1994. ISSN 0098-7484. doi:10.1001/jama.1994.03520100096046. URL <https://doi.org/10.1001/jama.1994.03520100096046>.
- [9] Xia-an Bi, Yang Wang, Qing Shu, Qi Sun, and Qian Xu. Classification of Autism Spectrum Disorder Using Random Support Vector Machine Cluster. *Frontiers in Genetics*, 9, 2018. ISSN 1664-8021. URL <https://www.frontiersin.org/articles/10.3389/fgene.2018.00018>.
- [10] Bernhard E. Boser, Isabelle M. Guyon, and Vladimir N. Vapnik. A training algorithm for optimal margin classifiers. In *Proceedings of the fifth annual workshop on Computational learning theory*, COLT '92, pages 144–152, New York, NY, USA, July 1992. Association for Computing Machinery. ISBN 978-0-89791-497-0. doi:10.1145/130385.130401. URL <https://dl.acm.org/doi/10.1145/130385.130401>.
- [11] Antonio Del Casale, Stefano Ferracuti, Alessandro Alcibiade, Sara Simone, Martina Nicole Modesti, and Maurizio Pompili. Neuroanatomical correlates of autism spectrum disorders: A meta-analysis of structural magnetic resonance imaging (MRI) studies. *Psychiatry Research. Neuroimaging*, 325:111516, September 2022. ISSN 1872-7506. doi:10.1016/j.psychresns.2022.111516.

- [12] Thomas P. DeRamus and Rajesh K. Kana. Anatomical likelihood estimation meta-analysis of grey and white matter anomalies in autism spectrum disorders. *NeuroImage : Clinical*, 7:525–536, November 2014. ISSN 2213-1582. doi:10.1016/j.nicl.2014.11.004. URL <https://www.ncbi.nlm.nih.gov/pmc/articles/PMC4375647/>.
- [13] A. Di Martino, C.-G. Yan, Q. Li, E. Denio, F. X. Castellanos, K. Alaerts, J. S. Anderson, M. Assaf, S. Y. Bookheimer, M. Dapretto, B. Deen, S. Delmonte, I. Dinstein, B. Ertl-Wagner, D. A. Fair, L. Gallagher, D. P. Kennedy, C. L. Keown, C. Keysers, J. E. Lainhart, C. Lord, B. Luna, V. Menon, N. J. Minshew, C. S. Monk, S. Mueller, R.-A. Müller, M. B. Nebel, J. T. Nigg, K. O’Hearn, K. A. Pelphrey, S. J. Peltier, J. D. Rudie, S. Sunaert, M. Thioux, J. M. Tyszka, L. Q. Uddin, J. S. Verhoeven, N. Wenderoth, J. L. Wiggins, S. H. Mostofsky, and M. P. Milham. The autism brain imaging data exchange: towards a large-scale evaluation of the intrinsic brain architecture in autism. *Molecular Psychiatry*, 19(6): 659–667, June 2014. ISSN 1476-5578. doi:10.1038/mp.2013.78. URL <https://www.nature.com/articles/mp201378>. Number: 6 Publisher: Nature Publishing Group.
- [14] Christine Ecker. The neuroanatomy of autism spectrum disorder: An overview of structural neuroimaging findings and their translatability to the clinical setting. *Autism*, 21(1):18–28, January 2017. ISSN 1362-3613. doi:10.1177/1362361315627136. URL <https://doi.org/10.1177/1362361315627136>. Publisher: SAGE Publications Ltd.
- [15] Christine Ecker, Vanessa Rocha-Rego, Patrick Johnston, Janaina Mourao-Miranda, Andre Marquand, Eileen M. Daly, Michael J. Brammer, Clodagh Murphy, and Declan G. Murphy. Investigating the predictive value of whole-brain structural mr scans in autism: A pattern classification approach. *NeuroImage*, 49(1):44–56, 2010. ISSN 1053-8119. doi:<https://doi.org/10.1016/j.neuroimage.2009.08.024>. URL <https://www.sciencedirect.com/science/article/pii/S1053811909009045>.

- [16] Anders Eklund, Thomas E. Nichols, and Hans Knutsson. Cluster failure: Why fMRI inferences for spatial extent have inflated false-positive rates. *Proceedings of the National Academy of Sciences*, 113(28):7900–7905, July 2016. doi:10.1073/pnas.1602413113. URL <https://www.pnas.org/doi/full/10.1073/pnas.1602413113>. Publisher: Proceedings of the National Academy of Sciences.
- [17] Thomas Martial Epalle, Yuqing Song, Zhe Liu, and Hu Lu. Multi-atlas classification of autism spectrum disorder with hinge loss trained deep architectures: ABIDE I results. *Applied Soft Computing*, 107:107375, August 2021. ISSN 1568-4946. doi:10.1016/j.asoc.2021.107375. URL <https://www.sciencedirect.com/science/article/pii/S1568494621002982>.
- [18] K. J. Friston, A. P. Holmes, K. J. Worsley, J.-P. Poline, C. D. Frith, and R. S. J. Frackowiak. Statistical parametric maps in functional imaging: A general linear approach. *Human Brain Mapping*, 2(4):189–210, 1994. ISSN 1097-0193. doi:10.1002/hbm.460020402. URL <https://onlinelibrary.wiley.com/doi/abs/10.1002/hbm.460020402>. eprint: <https://onlinelibrary.wiley.com/doi/pdf/10.1002/hbm.460020402>.
- [19] Karl Friston. Ten ironic rules for non-statistical reviewers. *NeuroImage*, 61(4):1300–1310, July 2012. ISSN 1053-8119. doi:10.1016/j.neuroimage.2012.04.018. URL <https://www.sciencedirect.com/science/article/pii/S1053811912003990>.
- [20] Phillip Good. *Permutation Tests*. Springer Series in Statistics. Springer, New York, NY, 2000. ISBN 978-1-4757-3237-5 978-1-4757-3235-1. doi:10.1007/978-1-4757-3235-1. URL <http://link.springer.com/10.1007/978-1-4757-3235-1>.
- [21] Ilaria Gori, Alessia Giuliano, Filippo Muratori, Irene Saviozzi, Piernicola Oliva, Raffaella Tancredi, Angela Cosenza, Michela Tosetti, Sara Calderoni, and Alessandra Retico. Gray Matter Alterations in Young Children with Autism Spectrum Disorders: Comparing Morphometry

at the Voxel and Regional Level. *Journal of Neuroimaging*, 25(6): 866–874, 2015. ISSN 1552-6569. doi:10.1111/jon.12280. URL <https://onlinelibrary.wiley.com/doi/abs/10.1111/jon.12280>. eprint: <https://onlinelibrary.wiley.com/doi/pdf/10.1111/jon.12280>.

- [22] J. M. Gorriz, C. Jimenez-Mesa, R. Romero-Garcia, F. Segovia, J. Ramirez, D. Castillo-Barnes, F. J. Martinez-Murcia, A. Ortiz, D. Salas-Gonzalez, I. A. Illan, C. G. Puntonet, D. Lopez-Garcia, M. Gomez-Rio, and J. Suckling. Statistical Agnostic Mapping: A framework in neuroimaging based on concentration inequalities. *Information Fusion*, 66:198–212, February 2021. ISSN 1566-2535. doi:10.1016/j.inffus.2020.09.008. URL <https://www.sciencedirect.com/science/article/pii/S1566253520303699>.
- [23] Juan M. Górriz, Javier Ramírez, F. Segovia, Francisco J. Martínez, Meng-Chuan Lai, Michael V. Lombardo, Simon Baron-Cohen, and John Suckling. A Machine Learning Approach to Reveal the NeuroPhenotypes of Autisms. *International Journal of Neural Systems*, 29(07):1850058, September 2019. ISSN 0129-0657. doi:10.1142/S0129065718500582. URL <https://www.worldscientific.com/doi/abs/10.1142/S0129065718500582>. Publisher: World Scientific Publishing Co.
- [24] Anibal Sólón Heinsfeld, Alexandre Rosa Franco, R. Cameron Craddock, Augusto Buchweitz, and Felipe Meneguzzi. Identification of autism spectrum disorder using deep learning and the ABIDE dataset. *NeuroImage : Clinical*, 17:16–23, August 2017. ISSN 2213-1582. doi:10.1016/j.nicl.2017.08.017. URL <https://www.ncbi.nlm.nih.gov/pmc/articles/PMC5635344/>.
- [25] Holly Hodges, Casey Fealko, and Neelkamal Soares. Autism spectrum disorder: definition, epidemiology, causes, and clinical evaluation. *Translational Pediatrics*, 9(Suppl 1):S55–S65, February 2020. ISSN 2224-4336. doi:10.21037/tp.2019.09.09. URL <https://www.ncbi.nlm.nih.gov/pmc/articles/PMC7082249/>.

- [26] Yun Jiao, Rong Chen, Xiaoyan Ke, Kangkang Chu, Zuhong Lu, and Edward H. Herskovits. Predictive models of autism spectrum disorder based on brain regional cortical thickness. *NeuroImage*, 50(2):589–599, April 2010. ISSN 1095-9572. doi:10.1016/j.neuroimage.2009.12.047.
- [27] Kyle B Jones, Kristina Cottle, Amanda Bakian, Megan Farley, Deborah Bilder, Hilary Coon, and William M McMahon. A description of medical conditions in adults with autism spectrum disorder: A follow-up of the 1980s Utah/UCLA Autism Epidemiologic Study. *Autism*, 20(5):551–561, July 2016. ISSN 1362-3613. doi:10.1177/1362361315594798. URL <https://doi.org/10.1177/1362361315594798>. Publisher: SAGE Publications Ltd.
- [28] Marcel Adam Just, Vladimir L. Cherkassky, Timothy A. Keller, and Nancy J. Minshew. Cortical activation and synchronization during sentence comprehension in high-functioning autism: evidence of underconnectivity. *Brain*, 127(8):1811–1821, August 2004. ISSN 0006-8950. doi:10.1093/brain/awh199. URL <https://doi.org/10.1093/brain/awh199>.
- [29] Meenakshi Khosla, Keith Jamison, Amy Kuceyeski, and Mert R. Sabuncu. Ensemble learning with 3D convolutional neural networks for functional connectome-based prediction. *NeuroImage*, 199:651–662, October 2019. ISSN 10538119. doi:10.1016/j.neuroimage.2019.06.012. URL <https://linkinghub.elsevier.com/retrieve/pii/S1053811919304963>.
- [30] Yazhou Kong, Jianliang Gao, Yunpei Xu, Yi Pan, Jianxin Wang, and Jin Liu. Classification of autism spectrum disorder by combining brain connectivity and deep neural network classifier. *Neurocomputing*, 324:63–68, January 2019. ISSN 09252312. doi:10.1016/j.neucom.2018.04.080. URL <https://linkinghub.elsevier.com/retrieve/pii/S0925231218306234>.
- [31] Anjali Krishnan, Lynne J. Williams, Anthony Randal McIntosh, and Hervé Abdi. Partial Least Squares (PLS) methods for neuroimaging: a tuto-

- rial and review. *NeuroImage*, 56(2):455–475, May 2011. ISSN 1095-9572. doi:10.1016/j.neuroimage.2010.07.034.
- [32] JANET E. Lainhart, JOSEPH Piven, MARYANN Wzorek, REBECCA Landa, SUSAN L. Santangelo, HILARY Coon, and SUSAN E. Folstein. Macrocephaly in Children and Adults With Autism. *Journal of the American Academy of Child & Adolescent Psychiatry*, 36(2):282–290, February 1997. ISSN 0890-8567. doi:10.1097/00004583-199702000-00019. URL <https://www.sciencedirect.com/science/article/pii/S0890856709628094>.
- [33] G. Li, K. Rossbach, W. Jiang, L. Zhao, K. Zhang, and Y. Du. Reduction in grey matter volume and its correlation with clinical symptoms in Chinese boys with low functioning autism spectrum disorder. *Journal of Intellectual Disability Research*, 63(2):113–123, 2019. ISSN 1365-2788. doi:10.1111/jir.12552. URL <https://onlinelibrary.wiley.com/doi/abs/10.1111/jir.12552>. eprint: <https://onlinelibrary.wiley.com/doi/pdf/10.1111/jir.12552>.
- [34] Alan J. Lincoln, Mark H. Allen, and Angela Kilman. The Assessment and Interpretation of Intellectual Abilities in People with Autism. In Eric Schopler and Gary B. Mesibov, editors, *Learning and Cognition in Autism*, pages 89–117. Springer US, Boston, MA, 1995. ISBN 978-1-4899-1286-2. doi:10.1007/978-1-4899-1286-2.6. URL https://doi.org/10.1007/978-1-4899-1286-2_6.
- [35] Michael V. Lombardo, Meng-Chuan Lai, and Simon Baron-Cohen. Big data approaches to decomposing heterogeneity across the autism spectrum. *Molecular Psychiatry*, 24(10):1435–1450, October 2019. ISSN 1476-5578. doi:10.1038/s41380-018-0321-0. URL <https://www.nature.com/articles/s41380-018-0321-0>. Number: 10 Publisher: Nature Publishing Group.
- [36] Matthew J. Maenner, Marshalyn Yeargin-Allsopp, Kim Van Naarden

- Braun, Deborah L. Christensen, and Laura A. Schieve. Development of a Machine Learning Algorithm for the Surveillance of Autism Spectrum Disorder. *PLOS ONE*, 11(12):e0168224, December 2016. ISSN 1932-6203. doi:10.1371/journal.pone.0168224. URL <https://journals.plos.org/plosone/article?id=10.1371/journal.pone.0168224>. Publisher: Public Library of Science.
- [37] Alessia Mammone, Marco Turchi, and Nello Cristianini. Support vector machines. *WIREs Computational Statistics*, 1(3):283–289, 2009. ISSN 1939-0068. doi:10.1002/wics.49. URL <https://onlinelibrary.wiley.com/doi/abs/10.1002/wics.49>. eprint: <https://onlinelibrary.wiley.com/doi/pdf/10.1002/wics.49>.
- [38] Anne Masi, Marilena M. DeMayo, Nicholas Glozier, and Adam J. Guastella. An Overview of Autism Spectrum Disorder, Heterogeneity and Treatment Options. *Neuroscience Bulletin*, 33(2):183–193, April 2017. ISSN 1995-8218. doi:10.1007/s12264-017-0100-y. URL <https://doi.org/10.1007/s12264-017-0100-y>.
- [39] Gráinne M. McAlonan, Vinci Cheung, Charlton Cheung, John Suckling, Grace Y. Lam, K. S. Tai, L. Yip, Declan G. M. Murphy, and Siew E. Chua. Mapping the brain in autism. A voxel-based MRI study of volumetric differences and intercorrelations in autism. *Brain: A Journal of Neurology*, 128(Pt 2):268–276, February 2005. ISSN 1460-2156. doi:10.1093/brain/awh332.
- [40] Laurent Mottron and Danilo Bzdok. Autism spectrum heterogeneity: fact or artifact? *Molecular Psychiatry*, 25(12):3178–3185, 2020. ISSN 1359-4184. doi:10.1038/s41380-020-0748-y. URL <https://www.ncbi.nlm.nih.gov/pmc/articles/PMC7714694/>.
- [41] Ahammed Ms, Niu S, Ahmed Mr, Dong J, Gao X, and Chen Y. Dark-ASDNet: Classification of ASD on Functional MRI Using Deep Neural

- Network. *Frontiers in neuroinformatics*, 15, June 2021. ISSN 1662-5196. doi:10.3389/fninf.2021.635657. URL <https://pubmed.ncbi.nlm.nih.gov/34248531/>. Publisher: Front Neuroinform.
- [42] Jared Nielsen, Brandon Zielinski, P Fletcher, Andrew Alexander, Nicholas Lange, Erin Bigler, Janet Lainhart, and Jeffrey Anderson. Multisite functional connectivity MRI classification of autism: ABIDE results. *Frontiers in Human Neuroscience*, 7, 2013. ISSN 1662-5161. URL <https://www.frontiersin.org/articles/10.3389/fnhum.2013.00599>.
- [43] William D. Penny, Karl J. Friston, John T. Ashburner, Stefan J. Kiebel, and Thomas E. Nichols. *Statistical Parametric Mapping: The Analysis of Functional Brain Images*. Elsevier, April 2011. ISBN 978-0-08-046650-7. Google-Books-ID: G_qdEsDlkp0C.
- [44] Fortunato Pesarin and Luigi Salmaso. The permutation testing approach: a review. *Statistica*, 70(4):481–509, December 2010. ISSN 1973-2201. doi:10.6092/issn.1973-2201/3599. URL <https://rivista-statistica.unibo.it/article/view/3599>. Number: 4.
- [45] J. Piven, S. Arndt, J. Bailey, S. Havercamp, N. C. Andreasen, and P. Palmer. An MRI study of brain size in autism. *The American Journal of Psychiatry*, 152(8):1145–1149, August 1995. ISSN 0002-953X. doi:10.1176/ajp.152.8.1145.
- [46] Joseph Piven, Eileen Nehme, Jon Simon, Patrick Barta, Godfrey Pearlson, and Susan E. Folstein. Magnetic resonance imaging in autism: measurement of the cerebellum, pons, and fourth ventricle. *Biological Psychiatry*, 31(5):491–504, March 1992. ISSN 0006-3223. doi:10.1016/0006-3223(92)90260-7. URL <https://www.sciencedirect.com/science/article/pii/0006322392902607>.
- [47] JOSEPH Piven, STEPHAN Arndt, JAMES Bailey, and NANCY Andreasen. Regional Brain Enlargement in Autism: A Magnetic Resonance Imaging Study. *Journal of the American Academy of Child*

- Journal of Adolescent Psychiatry*, 35(4):530–536, April 1996. ISSN 0890-8567. doi:10.1097/00004583-199604000-00020. URL <https://www.sciencedirect.com/science/article/pii/S0890856709635243>.
- [48] Faranak Rafiee, Roya Rezvani Habibabadi, Mina Motaghi, David M. Yousem, and Ilyssa J. Yousem. Brain MRI in Autism Spectrum Disorder: Narrative Review and Recent Advances. *Journal of magnetic resonance imaging: JMRI*, 55(6):1613–1624, June 2022. ISSN 1522-2586. doi:10.1002/jmri.27949.
- [49] Mladen Rakić, Mariano Cabezas, Kaisar Kushibar, Arnau Oliver, and Xavier Lladó. Improving the detection of autism spectrum disorder by combining structural and functional MRI information. *NeuroImage: Clinical*, 25:102181, January 2020. ISSN 2213-1582. doi:10.1016/j.nicl.2020.102181. URL <https://www.sciencedirect.com/science/article/pii/S221315822030019X>.
- [50] Pallavi Rane, David Cochran, Steven M. Hodge, Christian Haselgrove, David Kennedy, and Jean A. Frazier. Connectivity in Autism: A review of MRI connectivity studies. *Harvard review of psychiatry*, 23(4):223–244, 2015. ISSN 1067-3229. doi:10.1097/HRP.0000000000000072. URL <https://www.ncbi.nlm.nih.gov/pmc/articles/PMC5083037/>.
- [51] Kaitlin Riddle, Carissa J. Cascio, and Neil D. Woodward. Brain structure in autism: a voxel-based morphometry analysis of the Autism Brain Imaging Database Exchange (ABIDE). *Brain Imaging and Behavior*, 11(2):541–551, April 2017. ISSN 1931-7565. doi:10.1007/s11682-016-9534-5. URL <https://doi.org/10.1007/s11682-016-9534-5>.
- [52] Marion Rutherford, Karen McKenzie, Tess Johnson, Ciara Catchpole, Anne O’Hare, Iain McClure, Kirsty Forsyth, Deborah McCartney, and Aja Murray. Gender ratio in a clinical population sample, age of diagnosis and duration of assessment in children and adults with autism

- spectrum disorder. *Autism*, 20(5):628–634, July 2016. ISSN 1362-3613. doi:10.1177/1362361315617879. URL <https://doi.org/10.1177/1362361315617879>. Publisher: SAGE Publications Ltd.
- [53] Fermín Segovia. Sipba/sam: v1.0, February 2024. URL <https://doi.org/10.5281/zenodo.10616232>.
- [54] Fermín Segovia, Rosemary Holt, Michael Spencer, Juan M. Górriz, Javier Ramírez, Carlos G. Puntonet, Christophe Phillips, Lindsay Chura, Simon Baron-Cohen, and John Suckling. Identifying endophenotypes of autism: a multivariate approach. *Frontiers in Computational Neuroscience*, 8, 2014. ISSN 1662-5188. URL <https://www.frontiersin.org/articles/10.3389/fncom.2014.00060>.
- [55] Hidir Selcuk Nogay and Hojjat Adeli. Diagnostic of autism spectrum disorder based on structural brain MRI images using, grid search optimization, and convolutional neural networks. *Biomedical Signal Processing and Control*, 79:104234, January 2023. ISSN 1746-8094. doi:10.1016/j.bspc.2022.104234. URL <https://www.sciencedirect.com/science/article/pii/S1746809422006887>.
- [56] Zeinab Sherkatghanad, Mohammadsadegh Akhondzadeh, Soorena Salari, Mariam Zomorodi-Moghadam, Moloud Abdar, U. Rajendra Acharya, Reza Khosrowabadi, and Vahid Salari. Automated Detection of Autism Spectrum Disorder Using a Convolutional Neural Network. *Frontiers in Neuroscience*, 13, 2020. ISSN 1662-453X. URL <https://www.frontiersin.org/articles/10.3389/fnins.2019.01325>.
- [57] Liang Sun, Rinkal Patel, Jun Liu, Kewei Chen, Teresa Wu, Jing Li, Eric Reiman, and Jieping Ye. Mining Brain Region Connectivity for Alzheimer’s Disease Study via Sparse Inverse Covariance Estimation. volume 1335-1344, pages 1335–1344, June 2009. doi:10.1145/1557019.1557162.
- [58] P. Szatmari. Heterogeneity and the genetics of autism. *Journal of psychiatry & neuroscience: JPN*, 24(2):159–165, March 1999. ISSN 1180-4882.

- [59] N. Tzourio-Mazoyer, B. Landeau, D. Papathanassiou, F. Crivello, O. Etard, N. Delcroix, B. Mazoyer, and M. Joliot. Automated Anatomical Labeling of Activations in SPM Using a Macroscopic Anatomical Parcellation of the MNI MRI Single-Subject Brain. *NeuroImage*, 15(1):273–289, January 2002. ISSN 1053-8119. doi:10.1006/nimg.2001.0978. URL <https://www.sciencedirect.com/science/article/pii/S1053811901909784>.
- [60] Judith S. Verhoeven, Paul De Cock, Lieven Lagae, and Stefan Sunaert. Neuroimaging of autism. *Neuroradiology*, 52(1):3–14, January 2010. ISSN 1432-1920. doi:10.1007/s00234-009-0583-y. URL <https://doi.org/10.1007/s00234-009-0583-y>.
- [61] Xin Yang, Mohammad Samiul Islam, and A Khaled. *Functional connectivity magnetic resonance imaging classification of autism spectrum disorder using the multisite ABIDE dataset*. May 2019. doi:10.1109/BHI.2019.8834653. Pages: 4.
- [62] Xin Yang, Paul T. Schrader, and Ning Zhang. A Deep Neural Network Study of the ABIDE Repository on Autism Spectrum Classification. *International Journal of Advanced Computer Science and Applications (IJACSA)*, 11(4), June 2020. ISSN 2156-5570. doi:10.14569/IJACSA.2020.0110401. URL <https://thesai.org/Publications/ViewPaper?Volume=11&Issue=4&Code=IJACSA&SerialNo=1>. Number: 4 Publisher: The Science and Information (SAI) Organization Limited.
- [63] Li Zhang, Mingliang Wang, Mingxia Liu, and Daoqiang Zhang. A Survey on Deep Learning for Neuroimaging-based Brain Disorder Analysis, May 2020. URL <http://arxiv.org/abs/2005.04573>. arXiv:2005.04573 [cs, eess] version: 1.
- [64] W. Zhang, W. Groen, M. Mennes, C. Greven, J. Buitelaar, and N. Rommelse. Revisiting subcortical brain volume correlates of autism in the ABIDE dataset: effects of age and sex. *Psychological*

Medicine, 48(4):654–668, March 2018. ISSN 0033-2917, 1469-8978.
doi:10.1017/S003329171700201X. URL https://www.cambridge.org/core/product/identifier/S003329171700201X/type/journal_article.

- [65] Yu Zhao, Fangfei Ge, Shu Zhang, and Tianming Liu. 3D Deep Convolutional Neural Network Revealed the Value of Brain Network Overlap in Differentiating Autism Spectrum Disorder from Healthy Controls. In Alejandro F. Frangi, Julia A. Schnabel, Christos Davatzikos, Carlos Alberola-López, and Gabor Fichtinger, editors, *Medical Image Computing and Computer Assisted Intervention – MICCAI 2018*, Lecture Notes in Computer Science, pages 172–180, Cham, 2018. Springer International Publishing. ISBN 978-3-030-00931-1. doi:10.1007/978-3-030-00931-1_20.